Please find our point per point responses to each comment in bold

Response to interactive comment of Griet Neukermans

This paper provides a first description of the morphology, size, sinking speed, and dissolution of cryogenic gypsum crystals sampled in and under Arctic pack ice at four stations. These high-density crystals, precipitated during sea ice formation and released during ice melt, may potentially act as ballast mineral for organic material but have rarely been observed using traditional sampling methods due to difficulties of crystal preservation in samples (e.g. immediate dissolution in formaldehyde). Here, targeted crystal sampling was carried out for the first time in situ, in the bottom of sea ice, and with a plankton net on a ROV at 0m and 6m below the sea ice.
Correction: Sampling was carried out at 0, 5 and 10 m below the ice. See section Materials and Methods, line 133.

A detailed description of the sampled crystals is reported in this paper, including their morphology and size. Additional laboratory experiments were carried out to determine the sinking speed and dissolution conditions of the crystals. This work thus provides a first descriptive and quantitative sampling effort for cryogenic gypsum in the Arctic Ocean and I recommend publication of this work, but I have a number of major and minor comments that may help improve the paper.

Major comments:

1) This comment pertains to the potential ballast effect of cryogenic gypsum. The main motivation of this work is the potential ballast effect of cryogenic gypsum to help the sinking of organic matter through the Arctic water column. However, the excess density of cryogenic gypsum crystals derived from Equation 1 are very low, in the range 0.003-0.009 g cm-3. These values are in fact orders of magnitude lower than one would expect from the density of cryogenic gypsum; excess density = gypsum density– water density = 1.28 g cm-3. First, I think the reasons for the discrepancy between the expected and observed values should be better addressed. Second, an uncertainty assessment should be made on the measurements of particle diameter, sinking speed, and excess density. Third, how do these very low values of excess density of cryogenic crystals compare to the values of excess density of organic material? And are the excess density values of cryogenic gypsum high enough to provoke a ballast effect at all?

R1) These are very good points and we thank the reviewer for pointing them out. We have extensively discussed the issues raised on the excess density by you and reviewer 1 and decided to remove the plot with the excess density from the manuscript since it is just a calculation based on Stokes Law. We are confident that the actual measured settling velocities and crystal sizes are correct, however, Stokes Law is made for settling spheres with Reynolds Numbers much smaller than 1. Neither of these criteria are met for the gypsum crystals.
After going through the manuscript in great details, we are confident that by removing the excess density part of the story is not impacting the main conclusions or the supporting data to make those conclusions. The main point is that gypsum sinks very, very fast through the water column and will ballast settling aggregates if it is incorporated into the aggregates. This will increase the sinking velocities of the aggregates and provide a fast and stronger link between the surface ocean and the deep sea and seafloor. As it turned out, we have not used the excess densities in the discussion or the abstract, we were aware that

these data were based on approximations since there is no alternative to Stokes Law, which strictly does not apply to gypsum crystals. Therefore, we removed the excess densities from the manuscript, without the need to change the discussion or abstract.

We did test for porosity of the gypsum crystals to see if that could explain the low excess densities. We did this via SEM analyses on the crystals (all sites and size classes). We did not find any evidence for strongly increased porosities but found that the crystals looked solid. The large crystals had more complex structures and seemed to have increased surface roughness, but not to the extent that would explain the low excess densities. We therefore conclude that the results for the excess densities was because the gypsum crystals had high Reynolds numbers – at times larger than 100 – and were not spherical. The use of Stokes Law to calculate excess density is generally limited to spherical, non-permeable objects with Reynolds Numbers much smaller than 1.

2) Forth, a mineral material can only have a ballast effect on organic material if somehow the mineral gets associated with the organic material. Measuring sinking speed and density of a mineral alone does not prove its ballast effect. By which mechanisms could cryogenic gypsum get associated with organic material?

R2) When sea ice warms cryogenic gypsum can be released from widening brine channels and then fall directly in any organic material accumulating under the ice. This can be organic substances like exopolymer particels or algae. That way in Wollenburg et al. (2018) cryogenic gypsum was found to amount to >50% of collected *Phaeocystis* aggregates sinking from a prevailing *Phaeocystis* bloom. During PS106 no strong bloom was observed, but even the isolated *Melosira* alga collected from under the ice during this expedition showed entrained gypsum crystals. Comprehensive studies on this topic are scheduled for the coming months/expeditions. So far unpublished student tests with settling cylinders corroborate a significant ballasting effect of gypsum for cultured *Thalassiosira* algae.

3) This comment pertains to the hypothesized link between sea ice texture/porosity and cryogenic gypsum crystal size/morphology (section 4.1). This is certainly a very interesting hypothesis, but it is not clear at all how your results support it. This section needs improved clarity and better wording. The highly speculative nature of this entire section is obvious from the numerous occurrences of the words “likely”, “may”, “possibly”, etc.

R3) We agree with the reviewer that this section could be more precise, however when comparing cryogenic gypsum crystals sampled from the water column with crystals melted from ice cores that had been stored for > 1 year at -20°C the wording has to be cautious, since we do not know yet, how any storage or temperature change will affect the crystals. Thus, we feel it is more honest to keep any conclusion in comparing those results rather speculative.

4) Clarity could for example be improved by adding two rows at the top of Figure 3, one with a description of crystals in the ice core and one with a description of sea ice texture/porosity.

R4) Figure 3 relates to ROV net samples only. Storing the ice core for several months and melting the ice to obtain the gypsum crystals may, as has been discussed in the manuscript, have slightly altered the original crystal size/shape.

5) This work indicates a few of the reasons why cryogenic gypsum crystals have not been observed previously in scientific sampling efforts. I think the paper would benefit from a section of recommendations for future sampling.
R5) A sampling protocol is provided as S9 of the supplementary file.

6) Minor comments: L29: given the difficulty of showing association between mineral and organic material and the absence of this association in your results, I suggest you replace the word “indicated” by “suggested”.
R6) We have changed this passage accordingly.

7) L83: “to” should be “too”
R7) We have changed this passage accordingly.

8) L90: remove “best”
R8) We have changed this passage accordingly.

9) L103: insert “and” after “column”
R9) We have changed this passage accordingly.

10) L104: crystals (plural)
R10) We have changed this passage accordingly.

11) L106: the qualification of cryogenic gypsum as a ballast mineral is not demonstrated in this work in my opinion, as no association between gypsum and organic material has been clearly shown.
R11) As stated above, we found gypsum crystals adhering to *Melosira* alga, and in Wollenburg et al. (2018) comprising 50% of *Phaeocystis* aggregates, thus, gypsum can be incorporated in the two dominant Arctic alga and even in living *Melosira*. The experiments addressed the preservation potential and the sinking speed of single crystals of different shapes and sizes. The main aim here was to proof that gypsum crystals can actually sink to depth before being dissolved, which is crucial to proof its potential as ballast mineral.

12) L122: can you add a photo or sketch of the rov net?
R12) We have added such a photo as supplementary fig. 1 in the revised version.

13) Section 2.2: given all the sample handlings, the probability of crystal break up must be high?
R13) Not with the ROV net samples. The first author is a micropaleontologist that handled the samples with utmost care, and as almost no alga or plankton was observed in the samples, the actual sieving was very moderate.

14) Section 2.5: not clear how sinking speed was measured; did you have 2 cameras spaced 30 cm apart at the bottom and the top of the cylinder? What is the measure-C3ment uncertainty?
R14) The measurements were only done with one camera, so a two-dimensional view. We measured over a distance of ~5 cm after the crystals had reached terminal settling velocity and at stable and constant temperature and salinity. The technical uncertainties of the setup were smaller that the uncertainties between two similar sized gypsum crystals, which had up to 1000 m/d uncertainties (see figure 6 in the manuscript for crystals with equivalent spherical diameters of ~1 mm). We will add this respective information in the revised manuscript version

15) Section 2.6: You mention three tracking approaches. How did you combine them? Did you somehow average three different trajectories?
R15) As written in the manuscript, the reader is referred to Krumpen et al. 2019 (https://doi.org/10.1038/s41598-019-41456-y) for details on this approach.

16) L378: please report density in g cm-3 for consistency.
R16) We have changed this passage accordingly.

17) L409-413: What is the relevance of these sentences?
R17) It is just a description of what has been observed.

18) L524: Fig 2D refers to crystals collected at station 45, not 32/80.
R18) Correct. Fig. 8 refers to being close to stations 32/80. We will change the text to 'However, especially at the ice floe of station 32/80, we observed a high coverage of the ice underside by the filamentous algae *Melosira arctica*, and gypsum crystals were found in *M. arctica* filaments collected nearby (Fig. 8) as well as at station 45 (Fig. 2D)' from L499 onward in the revised version.

19) Fig 1: impossible to see the difference in trajectories 45 and 66.
R19) The starting point of each trajectory is indicated by a black, the end point by a respective white label. The trajectories are indeed close together. However, they are distinguishable by the colour-coding. The tracking of both ice floes started in the same month (July). Since the ice floe of Station 45 had a longer trajectory than Station 65, it had passed the position of Station 65 in March, which is why its trajectory was plotted in orange in that region. Following the colour scale of Figure 1 backwards, we can see that floe 45 made a circular turn in the Nansen Basin in winter 2016/17, but had actually been a 2-year floe probably originating from the Laptev Sea, whereas floe 66 probably formed in autumn 2016 in the Nansen Basin.

20) L789: with respect to Fig 7: please add your fitted curves to the figures.
R20) A regression line was added to the curves in the revised manuscript.

Response to Anonymous Referee #2

This is an excellently executed investigation on a subject that long has been around in the vertical flux literature. It is clearly and well written. I am not a chemical oceanographer
and can thus not evaluate most of the chemical analyses. However, the description of the morphology, size, dissolution nd sinking velocity of cryogenic gypsum particles is a major break-through for vertical flux regulation in ice-covered waters. When it comes to the regulation of vertical export of biogenic particles in the Arctic Ocean, in particular the sinking and non-sinking of phytoplankton and ice algae this manuscripts provides mechanisms that are of great interest. I would have liked to see some speculation in this direction. To the candidates that have been discussed
C1
previously belong Phaeocystis with sinks (1, 2) or does not (3). Similar speculations also exist for Melosira arctica. The authors may have the mechanism to understand the pelagic-benthic coupling in the Artic Ocean in their hands. This deserves some high-thinking. How will for example warming of surface waters below sea ice impact the sinking of biogenic matter and bloom development in the future?
(1) Wassmann, P., Vernet, M., Mitchell, G., Rey, P. (1990). Mass sedimentation of Phaeocystis pouchetii in the Barents Sea during spring. Mar. Ecol. Prog. Ser. 66: 183-195.
(2) Hamm, C., M. Reigstad, C. Wexels Riser, A. Mühlebach & P. Wassmann (2001). On

the trophic fate of Phaeocystis pouchetii: VII. Sedimentation of Phaeocystis-derived organic
matter via krill fecal strings during a Phaeocystis bloom in the Balsfjord, northern Norway. Mar. Ecol. Prog. Ser. 209: 55-69.
(3) Reigstad, M., Wassmann, P. (2007). Does Phaeocystis spp. contribute significantly to vertical export of biogenic matter? Biogeochemistry 83 (1-3): 217-234

Response to interactive comment by reviewer 2

Apart from being positive about the manuscript reviewer 2 asks for some speculative sentences on our finding in context to published papers on the fate of *Phaeocystis /Melosira* in carbon export, and to changes in the future Arctic Ocean. These suggestions conflict with the suggestions of reviewer 1 who requested to be less speculative. Furthermore, the question why a 'unsinkable alga' like *Phaeocystis* can sink once ballasted by cryogenic gypsum has also already been addressed by Wollenburg et al., 2018. We are continuing our research and will address these questions again with numbers and facts rather than to be just speculative in our next paper. As this manuscript is dedicated to what the titel says 'New observations of the distribution, morphology, and dissolution dynamics of cryogenic gypsum in the Arctic Ocean' we restrained from speculative outlooks on the future carbon pump.

Response to Editor decision 19_2_2020

The topic of your paper is timely and interesting. You provide original data which will be clearly beneficial to the community. The reviews are for the most part positive. I therefore encourage you to submit a revised version that I will review and possibly, but not necessarily, send again to reviewers. One issue that needs to be strengthened is the actual ballasting effect of the gypsum crystals. You morphological analysis clearly would benefit from a more elaborate aspect. For example, have you thought of measuring the specific surface area of the crystals to address the porosity issue? This would really be enlightening. An adequate method for this type of solid may be the BET method using methane adsorption. There is an appropriate system at PSI in Switzerland. Building your own system would probably be too time-consuming. I strongly suggest you explore this issue before submitting a revised version. I am ready to accept that such measurements cannot be done within the usual time frame for a revision, but please at least give it a try.

We have extensively discussed the issues raised on the excess density by you and reviewer 1 and decided to remove the plot with the excess density from the manuscript since it is just a calculation based on Stokes Law. We are confident that the actual measured settling velocities and crystal sizes are correct, however, Stokes Law is made for settling spheres with Reynolds Numbers much smaller than 1. Neither of these criteria are met for the gypsum crystals.
After going through the manuscript in great details, we are confident that by removing the excess density part of the story is not impacting the main conclusions or the supporting data to make those conclusions. The main point is that gypsum sinks very, very fast through the water column and will ballast settling aggregates if it is incorporated into the aggregates. This will increase the sinking velocities of the aggregates and provide a fast and stronger link between the surface ocean and the deep sea and seafloor. As it turned out, we have not used the excess densities in the discussion or the abstract, we were aware that these data were based on approximations since there

is no alternative to Stokes Law, which strictly does not apply to gypsum crystals. Therefore, we removed the excess densities from the manuscript, without the need to change the discussion or abstract.

We did test for porosity of the gypsum crystals to see if that could explain the low excess densities. We did this via SEM analyses on the crystals (all sites and size classes) and exemplified pictures are shown in S8 of the supplements of the revised manuscript. We did not find any evidence for strongly increased porosities but found that the crystals looked solid. The large crystals had more complex structures and seemed to have increased surface roughness, but not to the extent that would explain the low excess densities. We therefore conclude that the results for the excess densities was because the gypsum crystals had high Reynolds numbers – at times larger than 100 – and were not spherical. The use of Stokes Law to calculate excess density is generally limited to spherical, non-permeable objects with Reynolds Numbers much smaller than 1.

New observations of the distribution, morphology, and dissolution dynamics of cryogenic gypsum in the Arctic Ocean

Jutta E. Wollenburg[1*], Morten Iversen[1,2], Christian Katlein[1], Thomas Krumpen[1], Marcel Nicolaus[1], Giulia Castellani[1], Ilka Peeken[1], Hauke Flores[1]

[1]Alfred-Wegener-Institut Helmholtz-Zentrum für Polar- und Meeresforschung, D-27570, Bremerhaven, Germany

[2]MARUM and University of Bremen, D-27359, Bremen, Germany

[*]Corresponding author and requests for materials should be addressed to J.E.W. (email: Jutta.Wollenburg@awi.de)

Abstract

To date observations on a single location indicate that cryogenic gypsum ($Ca[SO_4]\cdot 2H_2O$) may constitute an efficient but hitherto overlooked ballasting mineral enhancing the efficiency of the biological carbon pump in the Arctic Ocean. In June-July 2017 we sampled cryogenic gypsum under pack-ice in the Nansen Basin north of Svalbard using a plankton net mounted on a Remotely Operated Vehicle (ROVnet). Cryogenic gypsum crystals were present at all sampled stations, which suggested a persisting cryogenic gypsum release from melting sea ice throughout the investigated area. This was supported by a sea-ice backtracking model indicating that gypsum release was not related to a specific region of sea ice formation. The observed cryogenic gypsum crystals exhibited a large variability in morphology and size, with the largest crystals exceeding a length of 1 cm. Preservation, temperature and pressure laboratory studies revealed that gypsum dissolution rates accelerated with increasing temperature and pressure, ranging from 6% d^{-1} by mass in Polar Surface Water (-0.5 °C) to 81% d^{-1} by mass in Atlantic Water (2.5 °C at 65 bar). When testing the preservation of gypsum in Formaldehyde-fixed samples we observed immediate dissolution. Dissolution at warmer temperatures and through inappropriate preservation media may thus explain why cryogenic gypsum was not observed in scientific samples previously. Direct measurements of gypsum crystal sinking velocities ranged between 200 and 7000 m d^{-1}, suggesting that gypsum-loaded marine aggregates could rapidly sink from the surface to abyssal depths, supporting the hypothesised potential of gypsum as a ballasting mineral in the Arctic Ocean.

Keywords:

Cryogenic gypsum, Arctic Ocean, mineral ballasting, biological carbon pump, sea ice.

Gelöscht:

Gelöscht: that indicated

Gelöscht: indicated

Gelöscht: .

1 Introduction

Climate change in the Arctic Ocean has led to a drastic reduction of summer sea ice extent as well as to a significant thinning of the sea ice (Kwok, 2018; Kwok and Rothrock, 2009). Sea ice strength has reduced, and increased deformation and fractionation result in a progressively increasing sea ice drift speed (Docquier et al., 2017) and sea-ice export. Over the past decades the ice export via the Fram Strait alone has increased by 11% per decade during the productive spring and summer period (Smedsrud et al., 2017). An increasing amount of sea ice produced in the East Siberian and Laptev Sea melts over the adjacent continental slopes or in the central Arctic Ocean (Krumpen et al., 2019). Overall, the Arctic Ocean sea ice cover has shifted to a predominantly seasonal ice cover. However, although the majority of sea ice diminishes during late summer, the amount of sea ice produced in autumn to winter progressively increases (Kwok, 2018).

Large-scale transformations in the seasonal sea-ice cover impact the physical, chemical and biological dynamics of the sea ice-ocean system. However, especially the interactions of physical-chemical processes within the sea ice and pelagic to benthic biological processes have only received little attention. Of particular importance are poorly soluble minerals precipitated within the brine channels of sea ice which, once released, may ballast organic material sinking to the sea-floor. The changing icescape with more leads and the thinner Arctic sea ice allows increasing light penetration into the under-ice surface water (Katlein et al., 2015; Nicolaus et al., 2013; Nicolaus et al., 2012), supporting fast-growing and often massive under-ice phytoplankton blooms (Arrigo et al., 2012; Arrigo et al., 2014; Assmy et al., 2017). A recent study reported on a sudden export event of an under-ice bloom of the 'unsinkable alga' *Phaeocystis,* caused by the ballasting effect of cryogenic gypsum released from melting sea ice (Wollenburg et al., 2018a). This single event was the first and only report of cryogenic gypsum release in the Arctic Ocean. Moreover, this sea ice precipitation of cryogenic gypsum has never been recorded in Arctic sediments, sediment traps or other field studies.

When sea ice forms, the concentrations of dissolved ions in brine increase, and depending on the temperature of sea ice, a series of minerals (ikaite, mirabilite, hydrohalite, gypsum, hydrohalite, sylvite, $MgCl_2$, Antarcticite) precipitate (Butler, 2016; Butler and Kennedy, 2015; Geilfus et al., 2013; Golden et al., 1998; Wollenburg et al., 2018a). Once released into the ocean, gypsum is considered to be the most stable of the cryogenic precipitates (Butler et al.,

Gelöscht:

Gelöscht: 6% and

Gelöscht: as annual mean, and

Gelöscht: , respectively

Gelöscht:

Gelöscht: seems

2017; Strunz and Nickel, 2001). Sea ice-derived cryogenic gypsum was first described by Geilfus et al. (Geilfus et al., 2013), in a comprehensive work on the chemical, physical, and mineralogical aspects of its precipitation in experimental and natural sea ice off Greenland. According to FREZCHEM, a chemical–thermodynamic model that was developed to quantify aqueous electrolyte properties at sub-zero temperatures, cryogenic gypsum can precipitate at temperatures below –18 °C, and within a small temperature window between –6.5 and –8.5 °C (Geilfus et al., 2013; Marion et al., 2010; Wollenburg et al., 2018a). However, measurements on the stoichiometric solubility products showed that gypsum dynamics in ice–brine equilibrium systems strongly depend on the solubility and precipitation of hydrohalite and mirabilite (Butler, 2016; Butler et al., 2017). So far gypsum precipitation in experimental setups were only observed at temperatures between -7.1 and -8.2 °C, and not in the lower temperature range (Butler, 2016; Butler et al., 2017). Moreover, as Arctic sea ice rarely reaches temperatures lower than -18 °C, cryogenic gypsum is more likely precipitated within the higher temperature window in the Arctic Ocean (Wollenburg et al., 2018a).

A model applied to understand the gypsum release event of 2015 showed that the ice floe was too warm when it started to form and identified December to February as the most likely time span for gypsum precipitation (Wollenburg et al., 2018a). Due to the absence of a downward brine flux in this advanced phase of sea ice formation, gypsum crystals likely remain trapped in the ice until spring. In the absence of sufficient field observations gypsum release from sea ice is expected to peak at the beginning of the melting season, when sea ice warms to temperatures above -5 °C. This temperature marks the transition in the fluid transport capacities of sea ice allowing brine water and included crystals to be released into the water column (Golden et al., 1998). However, in lack of any extensive year-round field studies our knowledge depends on models, kinetics and two single field observations (Geilfus et al., 2013; Wollenburg et al., 2018a). There are no studies on sea ice-derived cryogenic gypsum crystal morphologies and its stability in seawater. It is unclear whether gypsum just precipitates during the assumed peak in December to February or whether it continues to grow in remaining brines during sea ice drift.

In this study, we systematically investigated the occurrence of cryogenic gypsum release from sea ice in spring 2017 with special emphasis on the morphological properties of the crystals. Varieties of cryogenic gypsum crystal morphologies are described and illustrated. The sampled gypsum crystals were further subjected to various laboratory experiments. Hereby, we investigated the dissolution behaviour over typical depth- and temperature ranges of the

Gelöscht:

Gelöscht: firstly

Gelöscht: flow

Gelöscht: to

Gelöscht: best

Gelöscht: from

Gelöscht: We therefore need more studies on the formation and release of cryogenic gypsum to assess its impact on biogeochemistry in the Arctic and sub-Arctic.

Gelöscht: overall appearance

Arctic water column and in Formaldehyde solution typically used for biological sampling preservation. We also made direct measurements of the size-specific sinking speed of individual gypsum crystals. These experiments were conducted to answer the question, why cryogenic gypsum has not previously been observed in field studies and if it qualifies as ballast mineral.

Gelöscht: ,
Gelöscht: in
Gelöscht: were investigated and
Gelöscht: crystal measured.

2 Material and Methods

2.1 Gypsum sampling with the ROVnet and on-board treatment

RV *Polarstern* expedition PS 106 (June-July 2017) in the early melting season gave the opportunity to systematically study the occurrence of cryogenic gypsum release and the morphological properties of gypsum crystals in the area north of Svalbard and on the Barents Sea shelf (Fig. 1A; Table 1).

Gelöscht: overall appearance
Gelöscht: the

Cryogenic gypsum was sampled from the upper 10 m of the under-ice water at four stations distributed throughout the expedition area (Fig. 1A; Table 1). The first part of the expedition (PS106/1) consisted of a drift study to the north of Svalbard, during which the vessel was anchored to an ice floe (station 32). This ice floe was revisited 6 weeks later at the end of the expedition (PS106/2) (station 80). During the second part of the expedition (PS106/2), cryogenic gypsum was collected over the western Barents Sea (station 45) and in the Nansen Basin to the north-east of Svalbard (station 66).

Gypsum crystals were sampled with a plankton net mounted on a remotely operated vehicle (ROVnet, Fig. S1). The ROVnet consists of a Polycarbonate frame with an opening of 40 cm by 60 cm, to which a zooplankton net with a mesh size of 500 μm was attached (Flores, 2018). For gypsum sampling, a handmade nylon net with an opening of 10 cm by 15 cm and a mesh size of 30 μm was mounted in the zooplankton net opening. The concentrated particulate material of the small nylon net was collected in a 2 L polyethylene bottle attached to the cod end of the net. A gauze-covered window in the cod-end bottle allowed seawater to drain off. Both nets were mounted on the aft end of a M500 (Ocean Modules, Sweden) observation class ROV carrying an extensive sensor suite described in Katlein et al. (Katlein

et al., 2017). After each ROVnet deployment, the nets were rinsed with ambient sea-water to concentrate the sample in the cod end of the net. The ROVnet sampled horizontal profiles in the water directly below the sea ice. Standard ROVnet profiles were conducted at the ice-water interface, at 5 m and at 10 m depth. The distance covered by each profile ranged between 300 and 600 m. At station 32, the 10 m profile was aborted due to technical failure, and at station 80 no 5 m profile was sampled due to time constraints, and the subsurface sample was discarded due to handling failure (Table 1).

The concentrated particulate material collected in the cod-end bottle of the gypsum sampling net was mixed with a sample equivalent volume of 98% ethanol, and stored at 4 °C until further analyses (Wollenburg et al., 2018a).

At ROVnet sampling stations, ice thickness was estimated through thickness drill holes with a tape measure. To characterize the properties of the ice floes sampled on the floe-wide scale, ice thickness surveys were conducted at each sampling station with a GEM2 (Geophex) electromagnetic induction ice-thickness sensor (Katlein et al., 2018).

2.2 Initial analyses of ROVnet samples

In the home laboratory the samples were rinsed onto a 32 μm mesh using fresh water. The samples were then oven-dried at 50°C for 20 hours. The remaining crystals were transferred into pre-weighed micropaleontological slides, and their weight was determined with a high-precision Sartorius SE2 ultra-microbalance. Under a Zeiss Axio Zoom V16 microscope, pictures were taken with an Axiocam 506 colour camera. We made both overview images of the whole sample and detailed images of individual crystals. From all samples and crystal morphologies, individual crystals were analysed using Raman microscopy, which confirmed that the crystals were gypsum (Wollenburg et al., 2018a). As in some samples both, very large and very small crystals (Figs. S3-S4) were observed, the >32 μm samples were dry-sieved over a 63 μm analysis sieve. The length and width of the cryogenic gypsum crystals in the size fractions >32<63 μm and >63 μm was determined with the software application ImageJ on 50 crystals in each sample and size fraction (Schneider et al., 2012) (Tab. 2).

2.3 Initial analyses of ice cores

At all ice stations, sea ice cores for archive purposes and for further measurement of bottom communities were drilled with a 9 cm diameter ice corer (Kovacs Enterprise) and stored at -

20°C (Peeken, 2018). One ice-core from station 80 and four bottom slices (10 cm) of ice-cores from station 45 were studied to investigate the gypsum crystal morphologies within sea ice. Each section was transferred into a measuring jug with lukewarm tap water for approx. two seconds, and then the jug was emptied over a 32 μm analysis sieve, and repeatedly refilled. This process was continued until all ice was melted. With the aid of a hand shower and a wash bottle the residue on the sieve was rinsed and transferred into a 30 μm mesh-covered funnel, dried and transferred into a micropaleontological picking tray for inspection and documentation. For storage, the residue was transferred into pre-weighed labelled micropaleontological slides.

2.4 Dissolution experiments

The aim of our dissolution experiments was to investigate the persistence of gypsum crystals against dissolution in the Arctic water column (water mass trials) and under common biological sample treatment (Formaldehyde trial).

Dissolution experiments were carried out on individual gypsum crystals collected from ROVnet samples. Hereby, 5 cryogenic gypsum crystals with different crystal morphologies, and from both size fractions were used in each reaction chamber. Before the start and after the termination of each experiment, pictures of the cryogenic gypsum crystals used were taken with an Axiocam 506 colour camera under a Zeiss Axio Zoom V16 microscope. The weight of the crystals before and after each treatment was determined with a high-precision Sartorius SE2 ultra-microbalance after they had been transferred into a pre-weighted silver boat. The experimental running time of each experiment was 24 hours.

2.4.1 Water mass trials

The experiments to simulate dissolution within the different water masses and hydrostatic pressure regimes of the Arctic Ocean were carried out with high-pressure chambers installed in a cooling table (Wollenburg et al., 2018b). With a high-pressure pump (ProStar218 Agilent Technologies), peak tubing, and multiple titanium valves a continuous isobaric and isocratic one-way seawater flow of 0.3 ml/min was directed through a set of four serially arranged high-pressure chambers each with an internal volume of 0.258 ml (Wollenburg et al., 2018b). This setup allowed for dissolution experiments at defined pressures and temperatures (Wollenburg et al., 2018b). For the experiments, we used sterile-filtered (0.2 µm mesh) North Sea water that was adjusted to a salinity of 34.98 by addition of 1 g Instant Ocean® sea salt

per L and psu-offset. The natural pH of 8.1 after equilibration to the refrigerator's atmosphere (at 2.5 °C and at atmospheric pressure), lowers to pH 8.05 at 2.5 °C at 150 bar (Culberson and Pytkowicx, 1968). Five experiments, with 4 high-pressure chambers were carried out. The Polar Surface (PSW) water corresponding experimental trial was running at -0.5 °C and 3 bar, the experimental Atlantic Water (AW) trial at +2.5 °C and 65 bar, and three experimental Deep Water trials were conducted at -1 °C and 100, 120 and 150 bar, respectively.

2.4.2 Formaldehyde trial

To study the effect of Formaldehyde treatment on cryogenic gypsum, the crystals were subjected to a Formaldehyde solution of 4% in seawater, which is commonly used to preserve biological samples. The stock solution consisted of 500 ml Formaldehyde concentration of 40%, 500 ml aqua dest. and 100 g hexamethylenetetramine, adjusted to a pH of 7.3-7.9. Aliquots of the 20% stock solution were added to the four-fold volume of artificial Arctic Ocean sea water to obtain a final concentration of 4%.

The Gypsum crystals were transferred into Falcon Tubes, and the 4% Formaldehyde solution was added. The Falcon tubes were then either stored at 3 °C, or at room temperature. After the experiments, the gypsum crystal-Formaldehyde suspension was washed with deionized water over a 10 μm mesh using a wash bottle, and dried on gauze. As in all formaldehyde trials all gypsum dissolved, no post-experimental weight was determined.

2.5 Size-specific settling velocities of gypsum

The size-specific sinking velocity of cryogenic gypsum was measured in a settling cylinder (Ploug et al., 2008). The cylinder (30 cm high and 5 cm in diameter) was filled with filtered seawater (salinity 32) and surrounded by a water jacket for thermal stabilization at 2 °C. The settling cylinder was closed at both ends, only allowing insertion of a wide-bore pipette at the top. Immediately before measurement, the gypsum was submerged into seawater with a salinity of 32 and a temperature of 2 °C, and then transferred to the settling cylinder with a wide-bore pipette. The gypsum crystals were allowed to sink out of the wide-bore pipette, which was centered in the cylinder. The descent of the crystals was recorded by a Basler 4 MPixel Ethernet camera equipped with a 25 mm fixed focal lens (Edmund Optics). The settling column was illuminated from the sides by a custom-made LED light source. The camera recorded 7 images per second as the gypsum crystals sank through the settling column. The measurements were only done with one camera, so a two-dimensional view. We measured over a distance of ~5 cm after the crystals had reached terminal settling velocity

Gelöscht: pellets

and at stable and constant temperature and salinity. The technical uncertainties of the setup were smaller that the uncertainties between two similar sized gypsum crystals, which had up to 1000 m/d uncertainties (see figure 6, with equivalent spherical diameters of ~1 mm). The setup was calibrated by recording a length scale before sinking velocity measurements. The size and settling of the individual gypsum crystals was determined with the image analysis software ImageJ. This was done by using the projected area of the crystals to calculate the equivalent spherical diameter and the distance traveled between the subsequent images to determine the sinking velocity of the individual crystals (Iversen et al., 2010)

We calculated the excess density ($\Delta\rho$) ($\Delta\rho$ = gypsum density – water density) of the crystal from the Stokes drag equation:

$$\Delta\rho = \frac{C_D \rho_w SV^2}{\frac{4}{3} g ESD} \quad (1)$$

where C_D is the dimensionless drag force (equation 2), ρ_w is the density of seawater (1.0256 g cm^{-3}, for a salinity of 32 at 2 °C), SV is the measured sinking velocity in cm s^{-1}, g is the gravitational acceleration of 981 cm s^{-2}, and ESD is the equivalent spherical diameter in cm. We calculated C_D using the drag equation for low Reynolds numbers (White, 1974):

$$C_D = \left(\frac{24}{Re}\right) + \left(\frac{6}{1+Re^{0.5}}\right) + 0.4 \quad (2)$$

where the Reynolds number (Re) was defined as

$$Re = SV\ ESD\ \frac{\rho_w}{\eta} \quad (3)$$

where η is the dynamic viscosity (1.7545×10^{-2} g cm^{-1} s^{-1} for a salinity of 32 at 2 °C). Equation 2 is valid up to a Reynolds number of 2x10^5 (Vogel and Beety, 1994). The gypsum crystals had Reynolds numbers ranging from 0.77 to 128.

2.6 Backtracking the sampled ice flows under which cryogenic gypsum was sampled

To determine sea ice drift trajectories of sampled sea ice we used a Lagrangian approach (IceTrack) that traces sea ice backward or forward in time using a combination of satellite-derived low resolution drift products. So far, IceTrack has been used in a number of

publications to examine sea ice sources, pathways, thickness changes and atmospheric processes acting on the ice cover (Damm et al., 2018{Peeken, 2018 #13678; Krumpen et al., 2016; Peeken et al., 2018). A detailed description is provided in Krumpen et al. (Krumpen et al., 2019).

Sea ice motion information was provided by different institutions, obtained from different sensors, and for different time intervals. In this study we applied a combination of three different products: (i) motion estimates based on a combination of scatterometer and radiometer data provided by the Center for Satellite Exploitation and Research (CERSAT (Girard-Ardhuin and Ezraty, 2012), (ii) the OSI-405-c motion product from the Ocean and Sea Ice Satellite Application Facility (OSISAF (Lavergne, 2016), and (iii) Polar Pathfinder Daily Motion Vectors from the National Snow and Ice Data Center (NSIDC (Tschudi et al., 2016).

The tracking approach works as follows: An ice parcel is traced backward or forward in time on a daily basis. Tracking is stopped if a) ice hits the coastline or fast ice edge, or b) ice concentration at a specific location drops below 50% and we assume the ice to be formed or melted. The applied sea ice concentration product was provided by CERSAT and was based on 85 GHz SSM/I brightness temperatures, using the ARTIST Sea Ice (ASI) algorithm.

3 Results

3.1 Presence and distribution of cryogenic gypsum under the investigated ice-floes

Based on backtracking (Krumpen, 2018) and sea ice observations, the sampled ice-floes had an age of 1 to 3 years (Fig. 1B) and were originating from the Siberian Sea (station 32/80), the Laptev Sea (station 45), and were more locally grown in the Nansen Basin (station 66). Whereas the mean sea ice thickness at the ROV survey stations ranged between 94 and 156 cm, the mean sea ice thickness of the investigated ice-floes estimated by an ice-thickness sensor surveys (Katlein et al., 2018) was 1.90 m for station 32, 1.00 m for station 45, and 1.80 m for stations 66 and 80 (Fig. 1A, Table 1). Despite the different origins and thicknesses of sea ice, cryogenic gypsum crystals were found at all stations and in all depth layers sampled with the ROVnet (Figs. 1A, B, Tab. 1). At all stations and sampling depths the samples were dominated by cryogenic gypsum, with a proportional dry weight of >96.5% in the 5 m-sample

at station 32, and with >99% in all other samples (Figs. 2, Figs. S2-S5). Other lithogenic particles, as often found in sea ice (Nürnberg et al., 1994), were essentially absent.

3.2 The morphology of cryogenic gypsum

The samples collected at station 32 were dominated by rounded, matte, solid cryogenic gypsum crystals with a mean length-width ratio of 1.40-1.76 (Tab. 2, S2). The proportional mass contribution of the smaller-sized crystals of the >30<63 μm size fraction increased with depth and outweighed the contribution of the >63 μm size fraction with 56.30%, and 66.28% for the 0 and 5 m water depth sample, respectively (Fig. 3). At 0 m, the mean length of the crystals was 68.46 μm in the >63 μm size fraction and 44.27 μm in the >30<63 μm fraction. At 5 m depth, crystal dimensions were similar, ranging at mean crystal lengths of 63.28 μm in the >63 μm, and 35.90 μm in the >30<63 μm size fraction, respectively.

At station 45, the crystals were mostly solid and for most part hyaline, rather than matte crystals as at station 32 (Figs. 2C-D, 6, S3). With decreasing weight proportion, the >63 μm size clearly dominated the 0, 5, and 10 m samples with 79.90, 73.39, and 66.14%, respectively. In the 0 m layer samples, mean crystal lengths were 114.18 μm in the >63 μm size fraction and 58.74 μm in the >30<63 μm size fraction (Tab. 2). At 5 m depth, we observed mean crystal lengths of 111 μm in the >63 μm size fractions, and 56.73 μm in the >30<63 μm fraction. The mean crystal lengths in the 10 m sample was 92.83 and 50.32 μm for the >63 and >30<63 μm size fraction, respectively. At station 45 the crystal length-width ratio varied between 1.37 and 1.98, measured in the >30<63 μm size fraction of the surface sample, and the >63 μm size fraction of the 10 m sample. The cryogenic gypsum crystals retrieved from the melted ice core drilled at this station were solid and hyaline. In size and shape they resembled the crystals of the 10 m layer at this station, with a mean crystal length of 114.2 μm, mean width of 57.2 μm, and a length-width ratio of 2 (Fig. 4).

At station 66, the crystals from 0 m water depth were dominated by large, pencil-like, hyaline and solid crystals with a mean crystal length of 1,355 μm and mean width of 415 μm in the dominating >63 μm fraction (99.25% mass) (Fig. 2B, S4, Tab. 2). These crystals with an average length-width ratio of 3.27 were found as isolated crystals, but very often also as inter-grown crystal rosettes with two to more than 10 individual crystals involved (Fig. S4; Tab. 2). The >30<63 μm size fraction (0.75% mass) was dominated by matte, whitish, rounded gypsum particles and tiny gypsum needles with a mean crystal length of 56.67 μm (Fig. S4, Tab. 2.). As at the other stations the weight proportion of the >63 μm size fraction

Gelöscht: S1-S4

Gelöscht: S1

Gelöscht: S2

Gelöscht: S3

Gelöscht: S3

Gelöscht: S3

significantly decreased from 99.25 in the 0 m, to 75.23 at 5 m, and 61.18% in the 10 m sample (Fig. 2). The size of cryogenic gypsum crystals collected from the 5 and 10 m layers was significantly smaller and predominantly composed of isolated small hyaline and euhedral gypsum needles. The length-width ratio ranged between 5.60 (5 m) and 4.37 (10 m) (Figs. 2A, S4, Tab. 2). In the 5 m layer sample, the mean crystal length was 411.42 μm in the >63 μm size fraction, and 62.03 μm in the >30<63 μm size fraction. The 10 m samples showed a mean crystal length of 101.40 μm in the >63, and 30.71 μm in the >30<63 μm size fraction (Tab. 2).

In the 10 m layer sample of station 80, large tabular gypsum crystals measuring up to 1 cm in length (mean length: 3,078 μm, mean width: 1,830 μm) dominated the >63 μm size fraction. Their average length-width ratio was 1.7. This size fraction contributed 89.1% of the gypsum mass (Figs. 5, S5, Tab. 2). The >30<63 μm size fraction was composed of fragments of these large crystals and few small gypsum needles. These often intergrown columnar crystals looked bladed, for most part also dented and with numerous cracks. Their mean length was 71.8 μm. The ice core retrieved from this station was very porous and broke into pieces of 9 to 11 cm. Cryogenic gypsum was retrieved from all these ice core sections and revealed a dominance of extraordinary large crystals (Figs. 5, S5), resembling the ROVnet samples from this station. The largest cryogenic gypsum crystals >6,000 μm (mean crystal length: 2,821 μm, mean width: 1,689 m) were retrieved from the top-most 8 cm ice core section, whereas, the maximum crystal size gradually decreased downcore (Fig. S5). The crystals themselves lacked sharp corners, and the large crystals had cavities inside, indicating an advanced stage of dissolution (Figs. 5C-D; S5).

Gelöscht: S3

Gelöscht: S4

Gelöscht: S4

Gelöscht: S4

Gelöscht: S4

3.3 Dissolution experiments

3.3.1 Experiments to simulate cryogenic gypsum dissolution within the Arctic water column

Our study area was characterized by the presence of three main water masses (Nikolopoulos et al., 2018; Rudels, 2015): 1) The Polar Surface Water (PSW) including the halocline, with a variable mean salinity of 32 and a temperature range of -1.8 to 0.0 °C, extended from the surface to maximum 100 m water depth (Nikolopoulos et al., 2018). 2) The Atlantic Water (AW) with a mean salinity of 34.4 to 34.7 and variable temperature of 0.0 to 4.7 °C in the

study area extended from below the PSW to 600-800 m water depth (Nikolopoulos et al., 2018). 3) The Eurasian Arctic Deep Water (EADW) fills the deep Eurasian Basin below the AW with a temperature range of <0 to -0.94 °C and a salinity of about 34.9 (Nikolopoulos et al., 2018).

The dissolution experiments carried out to simulate dissolution in the PSW were set to 3 bar, -0.5 °C. Over the 24 hours lasting PSW-simulating dissolution experiment, about 6% of the gypsum dissolved (Figs. 6, S6A, Tab. 3). In the AW experiment, the combination of positive temperatures (2.5 °C) and a pressure of 65 bar impacted the dissolution on the cryogenic gypsum crystals more than in any other seawater trial. More than 80% of the cryogenic gypsum crystals dissolved during the 24-hours experiment (Figs. 6, S6B, Tab. 3, S7, Tab. 3). Moreover, as dissolution mainly affects the crystal's surface, smaller gypsums crystals and those with increased surface roughness (S8C-D) were preferentially impacted by dissolution, whereas larger and solid crystals with smooth surface showed the lowest dissolution (). The EADW-simulating dissolution experiments set to a temperature of -0.5 °C showed a progressive cryogenic gypsum dissolution of 26, 58, and 62% with increasing pressure for the 100, 120 and 150 bar experiments, respectively (Figs. S8A-B).

Gelöscht: S5A

[1] nach unten verschoben:). The EADW-simulating dissolution experiments set to a temperature of -0.5 °C showed a progressive cryogenic gypsum dissolution of 26, 58, and 62% with increasing pressure for the 100, 120 and 150 bar experiments, respectively (Figs.

Gelöscht: 6, S5B, Tab. 3).

Gelöscht: Fig. S5B

[1] verschoben (Einfügung)

Gelöscht: 6, S6, Tab. 3).

3.3.2 Experiments to simulate cryogenic gypsum dissolution within Formaldehyde-treated biological samples

In the Formaldehyde experiments we exposed our set of cryogenic gypsum crystals to a Formaldehyde solution of 4%, which is commonly used to store pelagic samples from the Polar Oceans (Edler, 1979). Irrespective of the temperature at which the sample was stored, all gypsum dissolved within 24 hours.

3.4 Sinking velocities of gypsum crystals

The sinking velocity (*SV*) of the gypsum crystals increased with crystal size (Fig. 7). Small crystals with an equivalent spherical diameter (*ESD*) of 200 μm sank with 300 m d^{-1} while large gypsum crystals with ESDs of 2,000 to 2,500 μm sank with velocities of 5,000 to 7,000 m d^{-1}. The size to settling relationship was best described by a power function ($SV = 4239.9\ ESD^{0.839}$, $R^2 = 0.84$).

Gelöscht: 7A

Gelöscht: As the power function suggests, the settling velocity levelled off for the largest gypsum crystals (Fig. 7A). The observed excess density of all crystals was smaller than is expected from the density of gypsum (2310 kg/m³). For the visually non porous smaller crystals drag, the deviation of gypsum crystals from round particles, and dissolution may be the main reason for the calculated lower density.¶ However, plotting the excess density as a function of size (Fig. 7B) also showed that the excess density of the gypsum decreased with increasing crystal size. The microscopic images show that large crystals were more porous and had more complex shapes (Fig. S8 A-C) compared to the small crystals that were more spherical and less porous (Figs. 2, 4-5, S8 D). Hence, the flat settling to size relationship for large gypsum crystals (Fig. 7A), was essentially due to a combination of increased porosity causing decreasing excess density and increased drag due to the complex shapes of the large crystals.

4 Discussion

4.1 Distribution and morphology of cryogenic gypsum crystals

This study shows for the first time the wide-spread presence of cryogenic gypsum under melting Arctic sea ice of different origin. At all stations cryogenic gypsum dominated the sample fraction of particles >30 μm in Eurasian Basin surface waters, indicating a continuous cryogenic gypsum flux from melting sea ice over a period of six weeks. When designing the ROVnet for cryogenic gypsum sampling, we opted for the coarser >30 μm mesh to prohibit an overflow of the sampling container when running into a phytoplankton bloom. However, as Geilfus et al. (Geilfus et al., 2013) had observed gypsum crystals as small as 10 μm, we probably lost an unknown proportion of smaller gypsum crystals by the chosen sampling strategy. The gypsum crystals described from sea ice so far retrieved from only 3-days-old experimental and 30 cm thick natural sea ice off Greenland were small (crystal length max. 100 μm), planar euhedral gypsum crystals often intergrown or as rosettes (Geilfus et al., 2013). Similar, but larger (crystal length up to 1 mm), gypsum crystals were observed within *Phaeocystis* aggregates collected in the region of the present study (Wollenburg et al., 2018a). However, here we show that gypsum crystals exhibit a strong variability in size and morphology. Particularly large crystals were characterised by more complex shapes (Fig. 2, 5, S3-4) and increased surface roughness (Figs. S8C-D), compared to the small planar euhedral (Fig. 2A) and more spherical crystals (Fig. S8A-B). Euhedral crystal needles larger but otherwise similar to those described by Geilfus et al. (Geilfus et al., 2013) and Wollenburg et al. (Wollenburg et al., 2018a) dominated the >63 μm fraction collected at 5 and 10 m depths at station 66, and smaller crystals contributed especially to the >30<63 μm size fraction of the station's subsurface samples.

As cryogenic gypsum forms in sea ice brine pockets or channels, the size and morphology especially of large crystals is likely determined by sea ice texture and porosity during gypsum precipitation. Pursuing this hypothesis, the large and intergrown crystals collected from the 0 m layer at station 66, and the 10 m layer and ice-core at station 80, formed in highly branched granular sea ice (Lieb-Lappen et al., 2017; Weissenberger et al., 1992). In contrast, the small cryogenic gypsum needles reported by Geilfus et al. (Geilfus et al., 2013) and Wollenburg et al. (Wollenburg et al., 2018a), may have preferentially formed in columnar sea ice. Even sampling the same ice-floe (station 32 and 80), the appearance of the crystals changed. Possibly, a widening of the brine channels during the elapsed time (6 weeks)

Gelöscht: warming

Gelöscht: porosity

Gelöscht: S6A-C

Gelöscht: S6D

allowed a release of larger crystals at station 80 when compared to station 32. However, crystal growth during this elapsed period or lateral advection of large crystals cannot be excluded. Thus, detailed texture analyses on sea ice cores prior to sampling are needed to validate or reject hypotheses on a link between sea ice porosity and cryogenic gypsum crystal size and morphology and should be considered in future studies.

The sea ice microstructure dictating the formation of gypsum crystals in the brine matrix likely varied among ice-floes due to different ages, origins and drift trajectories (Fig. 1B). For example, station 66 was the only station where the sea ice likely formed over the central Nansen Basin only months before our study (Fig. 1B). The surface sample of station 66 had large intergrown hyaline star-shaped gypsum crystals that were observed at no other station. They also showed a considerably higher length-width ratio than crystals from second-year ice of stations 32/80 and 45 (Fig. 1B; Fig. 2). Accordingly, a close relationship between local sea ice properties and gypsum crystal morphology in the underlying water was evident from the comparison of gypsum crystals collected with the ROVnet with those retrieved from ice cores collected at two stations. The ice-core samples revealed cryogenic gypsum crystals that basically resembled the crystal morphologies collected from the water column at the same stations, indicating that the gypsum morphologies observed in the water column likely reflect the gypsum precipitation conditions and brine-channel structure of local ice-floes. The current understanding of mineral precipitation in supersaturated brines relies on ice-core analyses, sea ice brine- and experimental studies, and on mathematical modelling of the temperature window in which each mineral is likely to form (Butler et al., 2017; Marion et al., 2010). There are still many uncertainties regarding the precipitation and dissolution of gypsum within natural sea ice and during ice-core storage. Although the FREZCHEM model and Gitterman Pathway predict gypsum precipitation under defined conditions, only Geilfus et al. (Geilfus et al., 2013) and Butler et al. (Butler et al., 2017) succeeded in retrieving gypsum under such conditions, whereas others failed (Butler and Kennedy, 2015). According to the FREZCHEM model, cryogenic gypsum precipitates at temperatures of -6.2 to -8.5 °C and at temperatures <-18 °C (Geilfus et al., 2013; Wollenburg et al., 2018a). Accordingly, a storage temperature of -20 °C would allow the post-coring precipitation of gypsum from contained brines. However, in field and experimental studies cryogenic gypsum was so far only observed to precipitate in the -6.2 to -8.5 °C temperature window, even when treatments were conducted below -20 °C (Butler et al., 2017; Geilfus et al., 2013). Furthermore, the observed signs of dissolution on the large cryogenic gypsum crystals from the ice-core when compared

Gelöscht: these

519 to the sharp-edged crystals retrieved from the water column at station 80 indicate that
520 significant new precipitation of gypsum during storage did not occur, rather the opposite.

521 Apart from the growing conditions of gypsum crystals within sea ice, the size spectrum of
522 crystals retrieved from different depths in the water column likely was essentially altered by
523 the size-dependent sinking velocity of the crystals. Because the sinking velocity of large
524 cryogenic gypsum crystals is high the chance to catch large crystals with horizontal transects
525 directly under the ice should be lower compared to small crystals (Fig. 7A). Accordingly,
526 significant amounts of large cryogenic gypsum crystals were mainly sampled from the 0 m
527 layer where they could be scraped off the underside of the ice (see station 66, Tab. 2). In
528 contrast, smaller cryogenic gypsum crystals sink at lower velocities (Fig. 7A). Hence, the
529 large quantity of small-sized crystals retrieved in the deeper layers of station 66, and all layers
530 of station 32 and 45 likely were influenced by the accumulated gypsum release in this size-
531 fraction, whereas the rarer large crystals indicated the momentary release at these stations.
532 The extremely large crystals sampled at station 80 at 10 m depth probably indicated an on-
533 going flux event during rapid melting. According to our dissolution experiments, gypsum
534 dissolution within Arctic surface waters should only have a minor impact on the size
535 distribution of cryogenic gypsum crystals within the surface water. Besides vertical flux,
536 advection of gypsum crystals with surface currents may also have influenced the size-
537 distribution of gypsum crystals sampled in the water column.

538

539 **4.2 Reasons why cryogenic gypsum was rarely observed in past studies**

540

541 The small temperature range of the -6.2 to -8.5 °C window, which is also the only gypsum
542 precipitation temperature spectrum applicable in the Arctic Ocean, has been considered one
543 reason why gypsum was not detected in other studies (Butler and Kennedy, 2015; Wollenburg
544 et al., 2018a). Furthermore, the kinetics of gypsum precipitation was considered as too slow
545 for detection during experimental studies, and the amount of gypsum hard to verify versus
546 other sea ice precipitates that are quantitatively much more abundant, leading the focus
547 towards other sea ice precipitates (Butler and Kennedy, 2015; Geilfus et al., 2013). Although
548 cryogenic mirabilite and hydrohalite are three and twenty-two times more abundant than
549 gypsum, respectively (Butler and Kennedy, 2015), gypsum is the only sea ice precipitate that
550 survives for one to several days within the Arctic water column. Cryogenic gypsum
551 dissolution increases with increasing hydrostatic pressure and increasing temperatures (Fig.

6). However, well-preserved cryogenic gypsum crystals were retrieved from algae aggregates collected from 2,146 m water depth, suggesting that either the transport from the surface to this depth was very rapid or that dissolution was decreased and/or prevented once gypsum crystals were included within the matrix of organosulfur compound-rich aggregates (Wollenburg et al., 2018a). Yet, as seawater is usually undersaturated with respect to gypsum (Briskin and Schreiber, 1978a; Briskin and Schreiber, 1978b) and is shown by our dissolution experiments, disaggregation of organic aggregates would expose the gypsum to the seawater and dissolve any crystals making it to the deep ocean or seafloor likely within a few days. The same dissolution would occur within the sampling cups of sediment traps, explaining why gypsum has not been observed in those type of samples.

Our dissolution experiments showed that cryogenic gypsum can persist long enough in the cold polar surface water to be collected in measurable concentrations. The missing evidence of gypsum from past studies was likely due to the quick dissolution of gypsum crystals at higher temperatures and pressure dependence of dissolution kinetics, impeding the discovery of gypsum in sediment trap samples and on the sea-floor. In addition, Formaldehyde preservation leads to the immediate dissolution of gypsum, destroying any evidence of cryogenic gypsum in all kinds of biological samples including water column and net samples. Based on our experience with the PS106 expedition samples and the experiments presented here, we propose a standardized procedure for gypsum sampling in the field. This procedure is part of the standard operating protocol for gypsum samplind on the MOSAIC expedition (S 9).

4.3 Potential of cryogenic gypsum as a ballast of algae blooms

We found less than 6% dissolution of individual crystals in Polar Surface Water (PSW) per day. Thus, at depths immediately below the fluorescence maximum where a significant part of organic aggregates are formed (Iversen et al. 2010), the gypsum scavenging and ballasting of aggregates (Turner, 2015) is little affected by gypsum dissolution (Olli et al., 2007) (Fig. 6, Tab. 3). Incorporation of dense minerals into settling organic aggregates will increase their density and, therefore, the size-specific sinking velocities of the aggregates (Iversen and Ploug, 2010; Iversen and Robert, 2015; van der Jagt et al., 2018). The high sinking velocity of large gypsum crystals >1 mm (5,000-7,000 m d^{-1} (Fig. 7A)) could create strong hydrodynamic shear that might cause disaggregation of fragile algae aggregates (Olli et al., 2007). However, smaller gypsum crystals have been observed inside *Phaeocystis* aggregates collected at depths

Gelöscht:

Gelöscht: too,

below 2000 m (Wollenburg et al. 2018a). This shows that cryogenic gypsum is incorporated into organic aggregates and supports that gypsum can be an important ballast mineral of organic aggregates.

As chlorophyll concentrations in the surface water were mostly low (< 1 mg m^{-3}, H.F. unpublished data), a massive gypsum-mediated export of phytoplankton was unlikely during expedition PS106. However, especially at the ice floe of station 32/80, we observed a high coverage of the ice underside by the filamentous algae *Melosira arctica*, and gypsum crystals were found in *M. arctica* filaments collected nearby (Fig. 8) as well as at station 45 (Fig. 2D). This indicates a potential for rapid *M. arctica* downfall mediated by cryogenic gypsum, as soon as the algal filaments were released from the melting sea ice. Hence, ballasting by cryogenic gypsum may also have contributed to the mass export of *Melosira arctica* aggregates observed in 2012 (Boetius et al. 2013).

Gelöscht: This
Gelöscht: previous suggestions of
Gelöscht: as
Gelöscht: , such as *Phaeocystis* (Wollenburg et al., 2018a) by rather small crystals
Gelöscht: Figs.
Gelöscht: , 8
Formatiert: Schriftart: (Standard) Times, Englisch (Vereinigtes Königreich)

5 Conclusions

This study shows for the first time that gypsum released to the water at the onset of melt season in the Arctic Ocean causes a constant flux of gypsum over wide spread areas and over a long period of time (> six weeks). The morphological diversity of gypsum crystals retrieved from Arctic surface waters and ice-cores indicated a complex variety of precipitation and release processes as well as modifications during sea ice formation, the melt phase, and in the water column. In the fresh and cold Polar surface water, gypsum crystals persist long enough to act as an effective ballast on organic matter, such as phytoplankton filaments and marine snow.

References:

Arrigo, K. R., Perovich, D. K., Pickart, R. S., Brown, Z. W., van Dijken, G. L., Lowry, K. E., Mills, M. M., Palmer, M. A., Balch, W. M., Bahr, F., Bates, N. R., Benitez-Nelson, C., Bowler, B., Brownlee, E., Ehn, J. K., Frey, K. E., Garley, R., Laney, S. R., Lubelczyk, L., Mathis, J., Matsuoka, A., Mitchell, B. G., Moore, G. W. K., Ortega-Retuerta, E., Pal, S., Polashenski, C. M., Reynolds, R. A., Schieber, B., Sosik, H. M., Stephens, M., and Swift, J. H.: Massive Phytoplankton Blooms Under Arctic Sea Ice, Science, 336, 1408, 2012.

Arrigo, K. R., Perovich, D. K., Pickart, R. S., Brown, Z. W., van Dijken, G. L., Lowry, K. E., Mills, M. M., Palmer, M. A., Balch, W. M., Bates, N. R., Benitez-Nelson, C. R., Brownlee, E., Frey, K. E., Laney, S. R., Mathis, J., Matsuoka, A., Greg Mitchell, B., Moore, G. W. K., Reynolds, R. A.,

631 Sosik, H. M., and Swift, J. H.: Phytoplankton blooms beneath the sea ice in the Chukchi sea,
632 Deep Sea Research Part II: Topical Studies in Oceanography, 105, 1-16, 2014.
633 Assmy, P., Fernández-Méndez, M., Duarte, P., Meyer, A., Randelhoff, A., Mundy, C. J., Olsen,
634 L. M., Kauko, H. M., Bailey, A., Chierici, M., Cohen, L., Doulgeris, A. P., Ehn, J. K., Fransson, A.,
635 Gerland, S., Hop, H., Hudson, S. R., Hughes, N., Itkin, P., Johnsen, G., King, J. A., Koch, B. P.,
636 Koenig, Z., Kwasniewski, S., Laney, S. R., Nicolaus, M., Pavlov, A. K., Polashenski, C. M.,
637 Provost, C., Rösel, A., Sandbu, M., Spreen, G., Smedsrud, L. H., Sundfjord, A., Taskjelle, T.,
638 Tatarek, A., Wiktor, J., Wagner, P. M., Wold, A., Steen, H., and Granskog, M. A.: Leads in
639 Arctic pack ice enable early phytoplankton blooms below snow-covered sea ice, Scientific
640 Reports, 7, 40850, 2017.
641
642 Briskin, M. and Schreiber, B. C.: Authigenic gypsum in marine sediments, Marine Geology,
643 28, 37-49, 1978.
644
645 Butler, B.: Mineral dynamics in sea ice brines, PhD, Bangor, 184 pp., 2016.
646
647 Butler, B. M. and Kennedy, H.: An investigation of mineral dynamics in frozen seawater
648 brines by direct measurement with synchrotron X-ray powder diffraction, Journal of
649 Geophysical Research: Oceans, 120, 5686-5697, 2015.
650
651 Butler, B. M., Papadimitriou, S., Day, S. J., and Kennedy, H.: Gypsum and hydrohalite
652 dynamics in sea ice brines, Geochimica et Cosmochimica Acta, 213, 17-34, 2017.
653
654 Culberson, C. and Pytkowicx, R. M.: Effect of pressure on carbonic acid, boric acid, and the
655 pH in seawater, Limnology and Oceanography, 13, 403-417, 1968.
656
657 Damm, E., Bauch, D., Krumpen, T., Rabe, B., Korhonen, M., Vinogradova, E., and Uhlig, C.:
658 The Transpolar Drift conveys methane from the Siberian Shelf to the central Arctic Ocean,
659 Scientific Reports, 8, 4515, 2018.
660
661 Docquier, D., Massonnet, F., Barthélemy, A., Tandon, N. F., Lecomte, O., and Fichefet, T.:
662 Relationships between Arctic sea ice drift and strength modelled by NEMO-LIM3.6, The
663 Cryosphere, 11, 2829-2846, 2017.
664
665 Edler, L.: Recommendations on Methods for Marine Biological Studies in the Baltic Sea:
666 Phytoplankton and chlorophyll, Department of Marine Botany, University of Lund, 1979.
667
668 Flores, H. E., J.; Lange, B.; Sulanke, E.; Niehoff, B.; Hildebrandt, N.; Doble, M.; Schaafsma, F.;
669 Meijboom, A.; Fey, B.; Kühn, S.; Bravo-Rebolledo; E.; Dorssen, M. van; Grandinger, R.;
670 Hasset, B.; Kunisch, E.; Kohlbach, D.; Graeve, M.; Franeker, J. A. van; Gradinger, Bluhm, B.:
671 Under-ice fauna, zooplankton and endotherms. In: The Expeditions PS106/1 and 2 of the
672 Research Vessel Polarstern to the Arctic Ocean in 2017, Macke, A. F., H. (Ed.), Reports on
673 polar and marine research, 2018.
674
675 Geilfus, N. X., Galley, R. J., Cooper, M., Halden, N., Hare, A., Wang, F., Søgaard, D. H., and
676 Rysgaard, S.: Gypsum crystals observed in experimental and natural sea ice, Geophysical
677 Research Letters, 40, 6362-6367, 2013.
678

679 Girard-Ardhuin, F. and Ezraty, R.: Enhanced Arctic Sea Ice Drift Estimation Merging
680 Radiometer and Scatterometer Data, IEEE Transactions on Geoscience and Remote Sensing,
681 50, 2639-2648, 2012.
682
683 Golden, K. M., Ackley, S. F., and Lytle, V. I.: The Percolation Phase Transition in Sea Ice,
684 Science, 282, 2238, 1998.
685
686 Iversen, M., Nowald, N., Ploug, H., A. Jackson, G., and Fischer, G.: High resolution profiles of
687 vertical particulate organic matter export off Cape Blanc, Mauritania: Degradation processes
688 and ballasting effects, Deep Sea Research Part I Oceanographic Research Papers, 57, 771-
689 784, 2010.
690
691 Iversen, M. H. and Ploug, H.: Ballast minerals and the sinking carbon flux in the ocean:
692 carbon-specific respiration rates and sinking velocity of marine snow aggregates,
693 Biogeosciences, 7, 2613-2624, 2010.
694
695 Iversen, M. H. and Robert, M. L.: Ballasting effects of smectite on aggregate formation and
696 export from a natural plankton community, Marine Chemistry, 175, 18-27, 2015.
697
698 Katlein, C., Arndt, S., Nicolaus, M., Perovich, D. K., Jakuba, M. V., Suman, S., Elliott, S.,
699 Whitcomb, L. L., McFarland, C. J., Gerdes, R., Boetius, A., and German, C. R.: Influence of ice
700 thickness and surface properties on light transmission through Arctic sea ice, Journal of
701 Geophysical Research: Oceans, 120, 5932-5944, 2015.
702
703 Katlein, C., Nicolaus, M., Sommerfeld, A., Copalorado, V., Tiemann, L., Zanatta, M., Schulz,
704 H., and Lange, B.: Sea Ice Physics. In: The Expeditions PS106/1 and 2 of the research vessel
705 Polarstern in the Arctic Ocean in 2017, Macke, A. F., H. (Ed.), Berichte zur Polarforschung
706 Bremerhaven, 2018.
707
708 Katlein, C., Schiller, M., Belter, H. J., Coppolaro, V., Wenslandt, D., and Nicolaus, M.: A New
709 Remotely Operated Sensor Platform for Interdisciplinary Observations under Sea Ice,
710 Frontiers in Marine Science, 4, 281, 2017.
711
712 Krumpen, T.: AWI ICETrack - Antarctic and Arctic Sea Ice Monitoring and Tracking Tool
713 Alfred-Wegener-Institut Hemholtz-Zentrum für Polar- und Meeresforschung, Bremerhaven,
714 Germany, 2018.
715
716 Krumpen, T., Belter, H. J., Boetius, A., Damm, E., Haas, C., Hendricks, S., Nicolaus, M., Nöthig,
717 E.-M., Paul, S., Peeken, I., Ricker, R., and Stein, R.: Arctic warming interrupts the Transpolar
718 Drift and affects long-range transport of sea ice and ice-rafted matter, Scientific Reports, 9,
719 5459, 2019.
720
721 Krumpen, T., Gerdes, R., Haas, C., Hendricks, S., Herber, A., Selyuzhenok, V., Smedsrud, L.,
722 and Spreen, G.: Recent summer sea ice thickness surveys in Fram Strait and associated ice
723 volume fluxes, The Cryosphere, 10, 523-534, 2016.
724
725 Kwok, R.: Arctic sea ice thickness, volume, and multiyear ice coverage: losses and coupled
726 variability (1958–2018), Environmental Research Letters, 13, 105005, 2018.

727
728 Kwok, R. and Rothrock, D. A.: Decline in Arctic sea ice thickness from submarine and ICESat
729 records: 1958-2008, Geophys. Res. Lett., 36, 2009.
730
731 Lavergne, T.: Validation and Monitoring of the OSI SAF Low Resolution Sea Ice Drift Product
732 (v5), 2016.
733
734 Lieb-Lappen, R. M., Golden, E. J., and Obbard, R. W.: Metrics for interpreting the
735 microstructure of sea ice using X-ray micro-computed tomography, Cold Regions Science and
736 Technology, 138, 24-35, 2017.
737
738 Marion, G. M., Mironenko, M. V., and Roberts, M. W.: FREZCHEM: A geochemical model for
739 cold aqueous solutions, Computers & Geosciences, 36, 10-15, 2010.
740
741 Nicolaus, M., Arndt, S., Katlein, C., Maslanik, J., and Hendricks, S.: Correction to "Changes in
742 Arctic sea ice result in increasing light transmittance and absorption", Geophysical Research
743 Letters, 40, 2699-2700, 2013.
744
745 Nicolaus, M., Katlein, C., Maslanik, J., and Hendricks, S.: Changes in Arctic sea ice result in
746 increasing light transmittance and absorption, Geophysical Research Letters, 39, 2012.
747
748 Nikolopoulos, A., Heuzé, C., Linders, T., Andrée, E., and Sahlin, S.: Physical Oceanography. In:
749 The Expeditions PS106/1 and 2 of the Research Vessel POLARSTERN to the Arctic Ocean in
750 2017, Macke, A. and Flores, H. (Eds.), Reports on Polar and Marine Research, Alfred-
751 Wegener Institute Helmholtz Centre for Polar and marine research, Bremerhaven, 2018.
752
753 Nürnberg, D., Wollenburg, I., Dethleff, D., Eicken, H., Kassens, H., Letzig, T., Reimnitz, E., and
754 Thiede, J.: Sediments in Arctic sea ice: Implications for entrainment, transport and release,
755 Marine Geology, 119, 185-214, 1994.
756
757 Olli, K., Wassmann, P., Reigstad, M., Ratkova, T. N., Arashkevich, E., Pasternak, A., Matrai, P.
758 A., Knulst, J., Tranvik, L., Klais, R., and Jacobsen, A.: The fate of production in the central
759 Arctic Ocean - top-down regulation by zooplankton expatriates?, Progress In Oceanography,
760 72, 84-113, 2007.
761
762 Peeken, I., Primpke, S., Beyer, B., Gütermann, J., Katlein, C., Krumpen, T., Bergmann, M.,
763 Hehemann, L., and Gerdts, G.: Arctic sea ice is an important temporal sink and means of
764 transport for microplastic, Nature Communications, 9, 1505, 2018.
765
766 Peeken, I. C., G.; Flores, H.; Ehrlich, J.; Lange, B.; Schaafsma, F., Gradinger, R.; Hassett, B.;
767 Kunisch, E.; Damm, E.; Verdugo, J.; Kohlbach, D.; Graeve, M.; Bluhm, B.: Sea ice biology and
768 biogeochemistry. In: The Expeditions PS106/1 and 2 of the Research Vessel Polarstern to the
769 Arctic Ocean in 2017, Macke, A. F., H. (Ed.), 719, Reports of polar and marine research, 2018.
770 Ploug, H., Iversen, M. H., Koski, M., and Buitenhuis, E. T.: Production, oxygen respiration
771 rates, and sinking velocity of copepod fecal pellets: Direct measurements of ballasting by
772 opal and calcite, Limnology and Oceanography, 53, 469-476, 2008.

Rudels, B.: Arctic Ocean circulation, processes and water masses: A description of observations and ideas with focus on the period prior to the International Polar Year 2007–2009, Progress in Oceanography, 132, 22-67, 2015.

Schneider, C. A., Rasband, W. S., and Eliceiri, K. W.: NIH Image to ImageJ: 25 years of image analysis, Nature Methods, 9, 671, 2012.

Smedsrud, L. H., Halvorsen, M. H., Stroeve, J. C., Zhang, R., and Kloster, K.: Fram Strait sea ice export variability and September Arctic sea ice extent over the last 80 years, The Cryosphere, 11, 65-79, 2017.

Strunz, H. and Nickel, E. H.: Strunz Mineralogical Tables. Chemical-structural Mineral Classification System, Schweizerbart'sche Verlagsbuchhandlung (Nägele u. Obermiller), Stuttgart, 2001.

Tschudi, S., Fowler, C., Maslanik, J., Stewart, J., and Stewart, W.: Polar Pathfinder Daily 25 km EASE-Grid Sea Ice Motion Vectors. In: Technical report, NASA National Snow and Ice Data Center Distributed Active Archive Center, Boulder, Colorado USA 2016.

Turner, J. T.: Zooplankton fecal pellets, marine snow, phytodetritus and the ocean's biological pump, Progress in Oceanography, 130, 205-248, 2015.

van der Jagt, H., Friese, C., Stuut, J.-B. W., Fischer, G., and Iversen, M. H.: The ballasting effect of Saharan dust deposition on aggregate dynamics and carbon export: Aggregation, settling, and scavenging potential of marine snow, Limnology and Oceanography, 63, 1386-1394, 2018.

Vogel, S. and Beety, S. T.: Life in Moving Fluids: The Physical Biology of Flow, Princeton University Press, 1994.

Weissenberger, J., Dieckmann, G., Gradinger, R., and Spindler, M.: Sea ice: A cast technique to examine and analyze brine pockets and channel structure, Limnology and Oceanography, 37, 179-183, 1992.

White, F. M.: Viscous fluid flow, McGraw-Hill, 1974. 614, 1974.

Wollenburg, J. E., Katlein, C., Nehrke, G., Nöthig, E. M., Matthiessen, J., Wolf- Gladrow, D. A., Nikolopoulos, A., Gázquez-Sanchez, F., Rossmann, L., Assmy, P., Babin, M., Bruyant, F., Beaulieu, M., Dybwad, C., and Peeken, I.: Ballasting by cryogenic gypsum enhances carbon export in a Phaeocystis under-ice bloom, Scientific Reports, 8, 7703, 2018a.

Wollenburg, J. E., Zittier, Z. M. C., and Bijma, J.: Insight into deep-sea life – Cibicidoides pachyderma substrate and pH-dependent behaviour following disturbance, Deep Sea Research Part I: Oceanographic Research Papers, 138, 34-45, 2018b.

Table captions:

Tab. 1: Properties of sea ice stations and characteristics of ROVnet profiles.

Cruise Site	Date	Latitude (Deg N)	Longitude (Deg E)	Ocean depth (m)	Sampling depth	Water temp. (°C)	Salinity	Mean ice thickness (m)	Filtered water volume (m^3)
PS106.1 Stat. 32	2017-06-15	81.73	10.86	1608	under-ice	-1.94	34.27	1.90	2.2
					5 m	n.a	n.a.	1.90	3.9
PS106.2 Stat. 45	2017-06-25	78.10	30.47	233	under-ice	-1.52	33.84	1.00	2.3
					5 m	-1.47	34.11	1.00	4.5
					10 m	-1.68	34.29	1.00	2.5
PS106.2 Stat. 66	2017-07-02	81.66	32.34	1506	under-ice	-1.67	33.18	1.80	3.1
					5 m	-1.71	33.76	1.80	2.7
					10 m	-1.73	33.78	1.80	3.1
PS106.2 Stat. 80	2017-07-12	81.37	17.13	1010	10 m	-1.37	32.87	1.80	1.7

Formatiert: Schriftart: Nicht Fett

[2] verschoben (Einfügung)

Formatiert: Links

Formatierte Tabelle

Formatiert: Hochgestellt

[2] nach oben verschoben: Tab. 1: Properties of sea ice stations and characteristics of ROVnet profiles. ¶

827 Tab. 2: Size measurements and percentage of mass contribution of gypsum crystals from the
828 >63 μm size fraction and the >30 < 63 μm size fraction

	>63 µm fraction			>30<63 µm fraction				
Cruise, Site, mean water depth of the catch	Mean length µm	Mean width µm	length/ width ratio	Mean length µm	Mean width µm	length/ width ratio	>63 µm fraction weight%	>30<63 µm fraction weight%
PS106.1, Stat. 32, 0 m	68.46	44.27	1.55	50.64	35.03	1.45	43.70	56.30
PS106.1, Stat. 32, 5 m	63.28	35.90	1.76	49.91	35.57	1.40	33.72	66.28
PS106.1, Stat. 32, mean (0-5 m)	65.87	40.09	1.64	50.28	35.30	1.42	38.71	61.29
PS106.2, Stat. 45, 0 m	114.18	65.93	1.73	58.74	42.84	1.37	79.90	20.10
PS106.2, Stat. 45, 5 m	110.98	64.84	1.71	56.73	38.89	1.46	73.39	26.61
PS106.2, Stat. 45 , 10 m	92.83	46.81	1.98	50.32	29.98	1.68	66.14	33.86
PS106.2, Stat. 45, mean (0-10 m)	85.49	44.45	1.92	77.93	24.28	3.21	73.14	26.86
PS106.2, Stat. 66, 0 m	1355.38	415.10	3.27	56.67	25.63	2.21	99.25	0.75
PS106.2, Stat. 66, 5 m	411.42	73.45	5.60	62.03	12.20	5.08	75.23	24.77
PS106.2, Stat. 66, 10 m	101.40	23.19	4.37	30.71	5.79	5.30	61.18	38.82
PS106.2, Stat. 66, mean (0-10 m)	599.17	164.78	3.64	59.96	12.61	4.76	58.16	41.84
PS106.2, Stat. 80, 10 m	3078.44	1830.00	1.68	71.78	30.76	2.33	89.05	10.95

829

830

831

Gelöscht:

	>63 µm fraction	
Cruise, Site, mean water depth of the catch	Mean length µm	Mean width µm
PS106.1, Stat. 32, 0 m	68.46	44.27
PS106.1, Stat. 32, 5 m	63.28	35.90
PS106.1, Stat. 32, mean (0-5 m)	65.87	40.09
PS106.2, Stat. 45, 0 m	114.18	65.93
PS106.2, Stat. 45, 5 m	110.98	64.84
PS106.2, Stat. 45 , 10 m	92.83	46.81
PS106.2, Stat. 45, mean (0-10 m)	85.49	44.45
PS106.2, Stat. 66, 0 m	1355.38	415.10
PS106.2, Stat. 66, 5 m	411.42	73.45
PS106.2, Stat. 66, 10 m	101.40	23.19
PS106.2, Stat. 66, mean (0-10 m)	599.17	164.78
PS106.2, Stat. 80, 10 m	3078.44	1830.00

Gelöscht: ¶ ... [1]

Formatiert: Abstand Nach: 10 Pt., Zeilenabstand: Mehrere 1.15 ze

Tab. 3: Dissolution experiments on cryogenic gypsum crystals. 'Water mass' simulating experiments with 34.9‰ sterile filtered seawater. Each experiment was conducted in parallel in 3-4 separate pressure chambers.

	Dissolution in weight%				
Chamber (no.)/Water mass	PSW	AW	EADW (1)	EADW (2)	EADW (3)
1	11.34	76.22	47.52	57.08	74.92
2	1.33	86.23	26.09	71.03	53.77
3	8.29	82.93	21.05	47.15	57.43
4	2.99	78.57	10.91	58.56	
Mean	**5.99**	**80.77**	**26.39**	**58.34**	**62.04**

Formatiert: Schriftart: 12 Pt.

Formatiert: Schriftart: Nicht Fett

Figure captions:

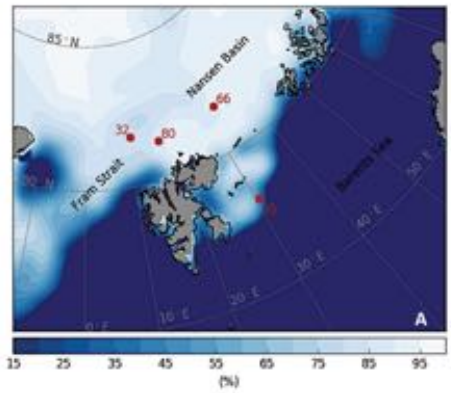
85° N
Nansen Basin
66
32
80
Fram Strait
Barents Sea
A
15
25
35
45
55
65
75
85
95
(%)

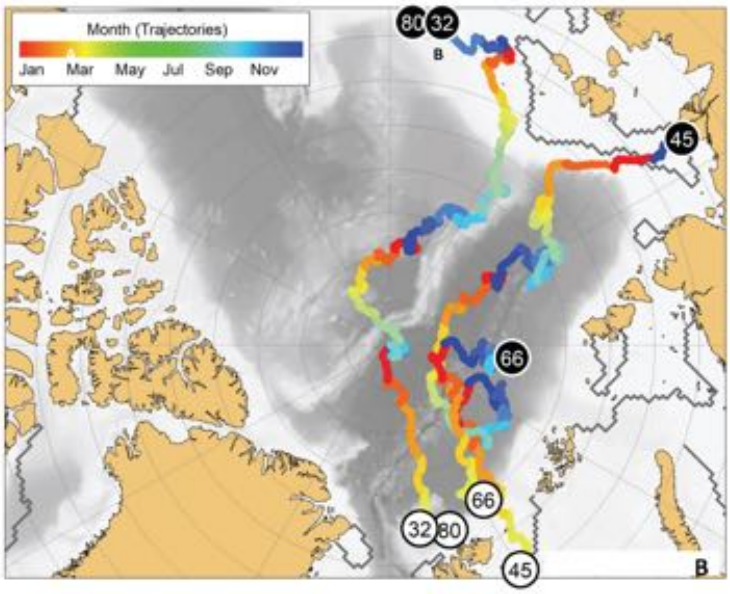
Month (Trajectories)
Jan
Mar
May
Jul
Sep
Nov
80
32
B
45
66
66
32
80
45
B

842

Gelöscht: Seitenumbruch

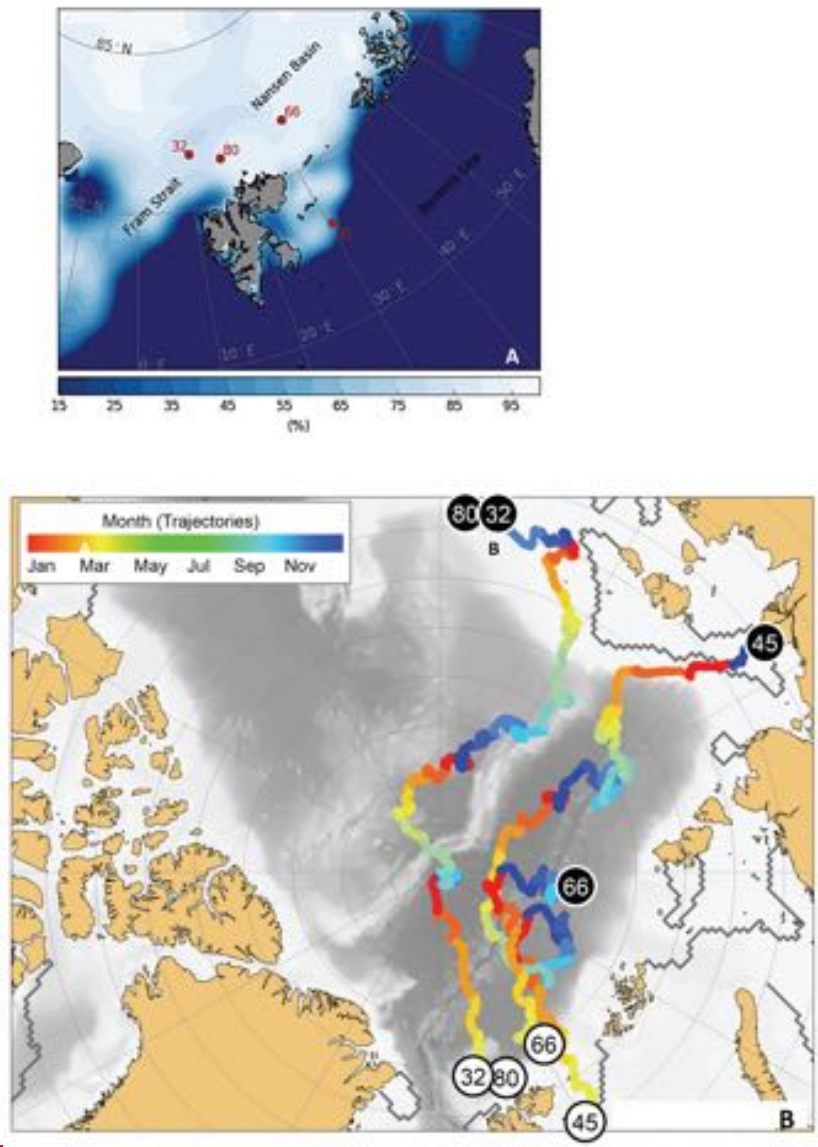

Fig. 1: Study area with sample locations. A: Sea ice coverage at the station and time of sampling in %. B) Trajectories of the sea ice from which the cryogenic gypsum was released. Each trajectory starts where sea ice formed (black circles), and shows its drift until the time

and place of sampling (white circles). The colour scale of the drift trajectories indicates the month in which the back-tracked sea ice was at any given position.

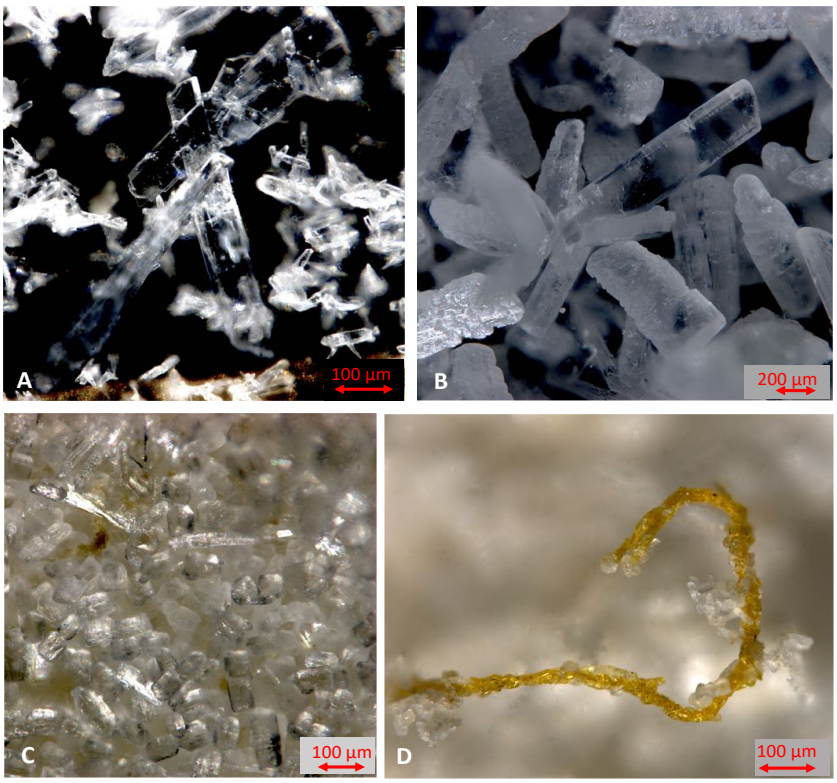

851

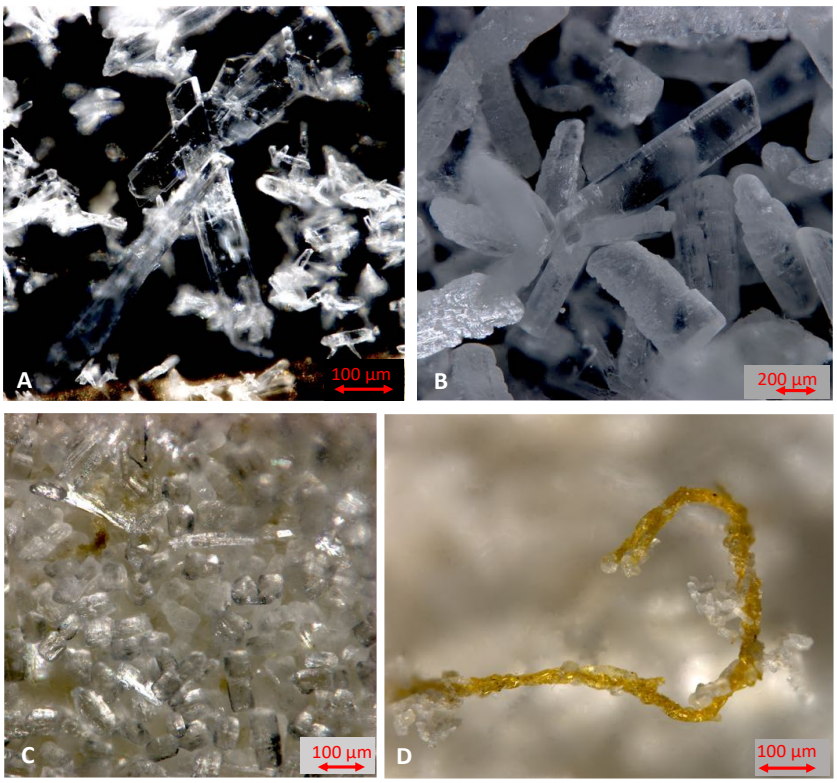

Fig. 2: Cryogenic gypsum crystals collected during Polarstern expedition PS106-1 from the upper water column. A) Crystals collected from station 66 at 5 m water depth. B) Crystals collected from station 66 at 0 m water depths. C) Crystals collected from station 45 at 10 m water depth. D) Crystals collected from station 45 at 10 m water depths entangled in an algae filament.

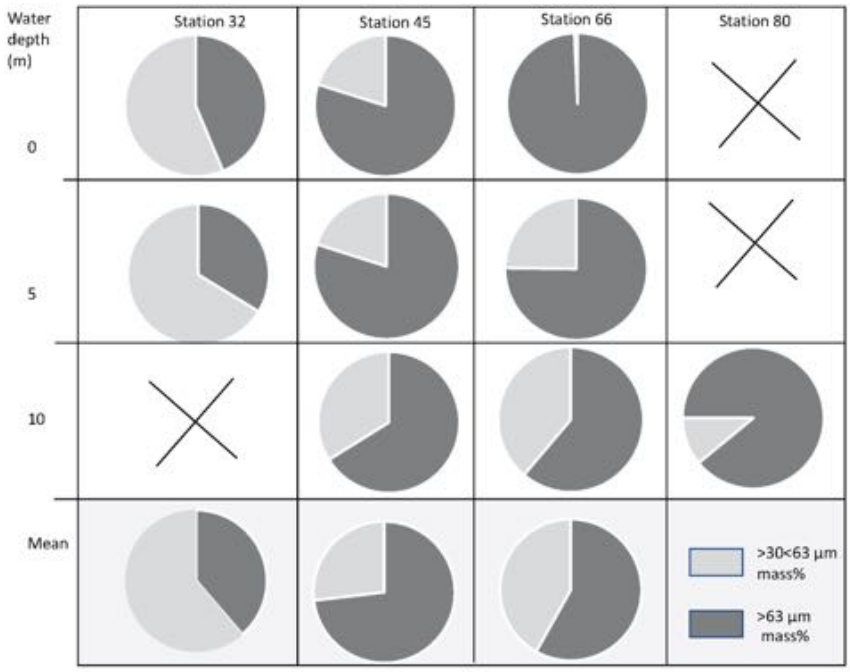
Water depth (m)
Station 32
Station 45
Station 66
Station 80
0
5
10
Mean
>30<63 µm mass%
>63 µm mass%

861

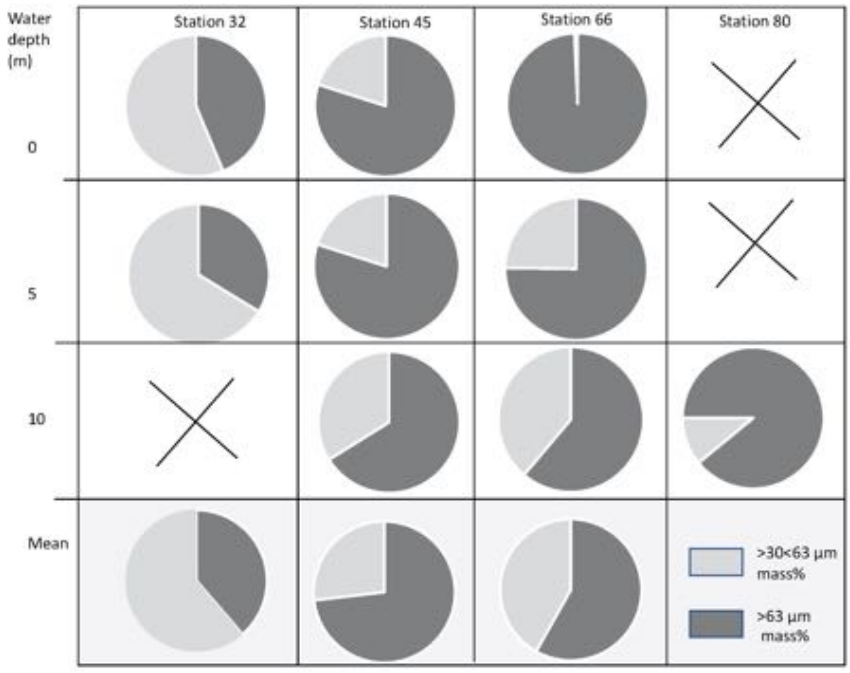
Water depth (m)
Station 32
Station 45
Station 66
Station 80
0
5
10
Mean
>30<63 µm mass%
>63 µm mass%

862

Fig. 3: Proportional mass (%) of cryogenic gypsum for the size fractions >30<63 μm and >63 μm for all ROV samples.

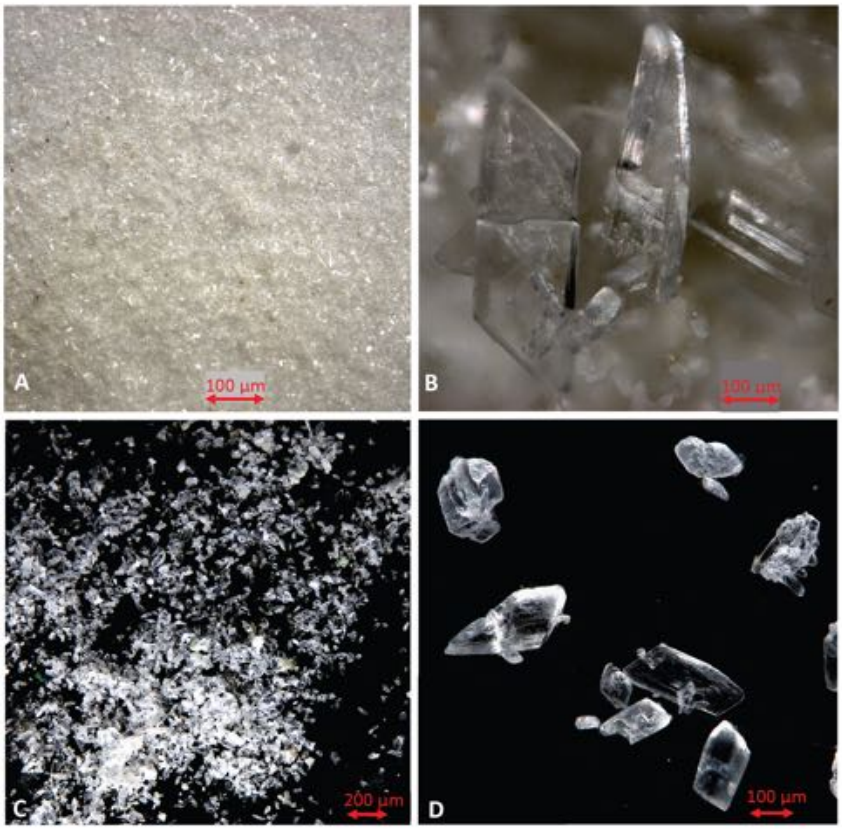

866

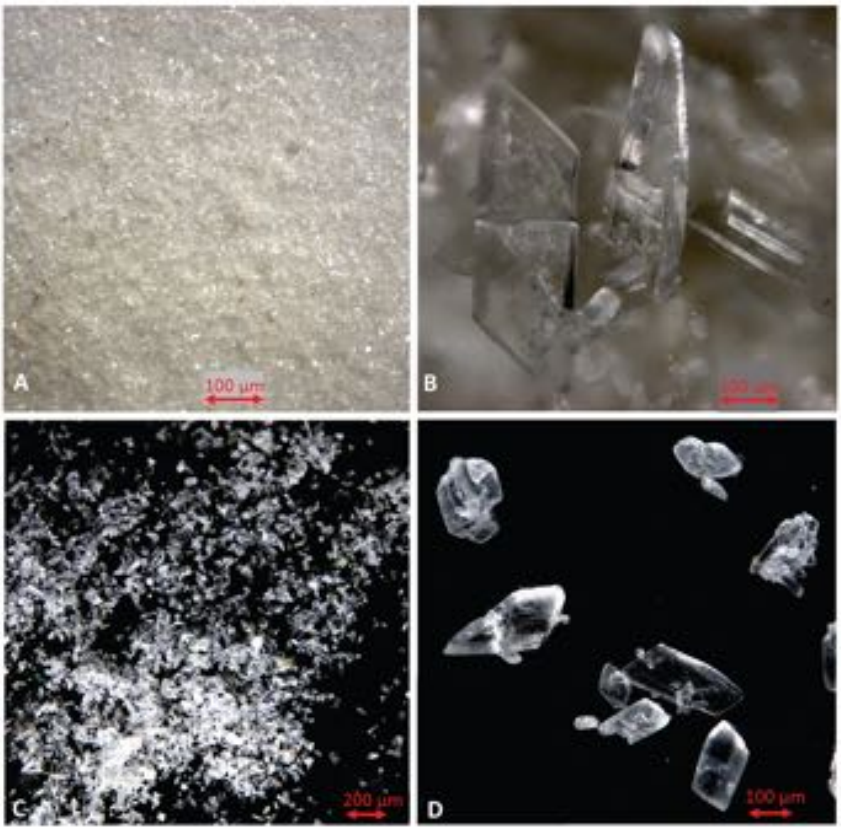

Fig. 4: Comparison of cryogenic gypsum crystals collected from the water column at station PS45 (10 m water depth) (A-B) with crystals retrieved from an ice-core collected above the ROVnet sampling area (C-D).

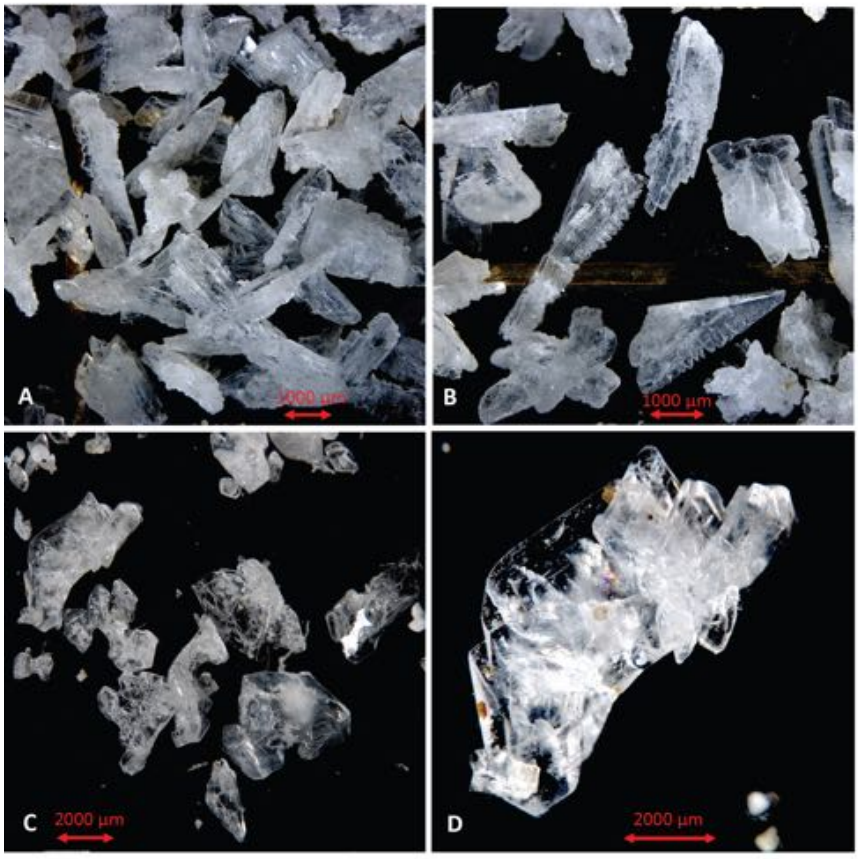

873

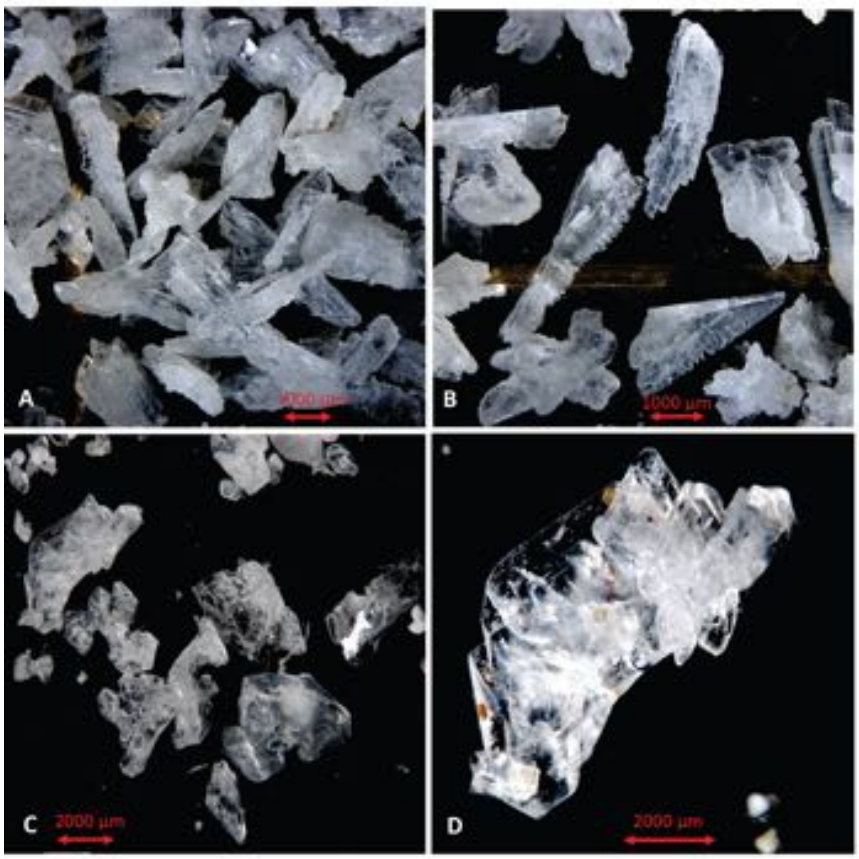

Fig. 5: Comparison of cryogenic gypsum crystals collected from the water column at station PS80-2 (10 m water depth) (A-B) with crystals retrieved from an ice-core collected above the ROVnet sampling area (C-D).

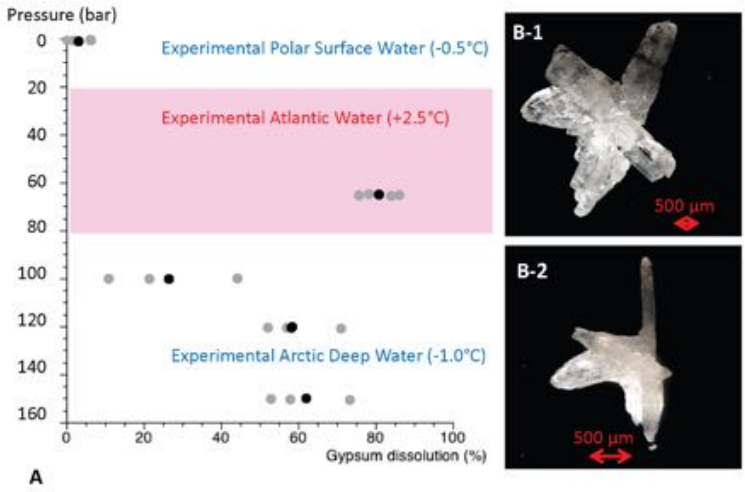

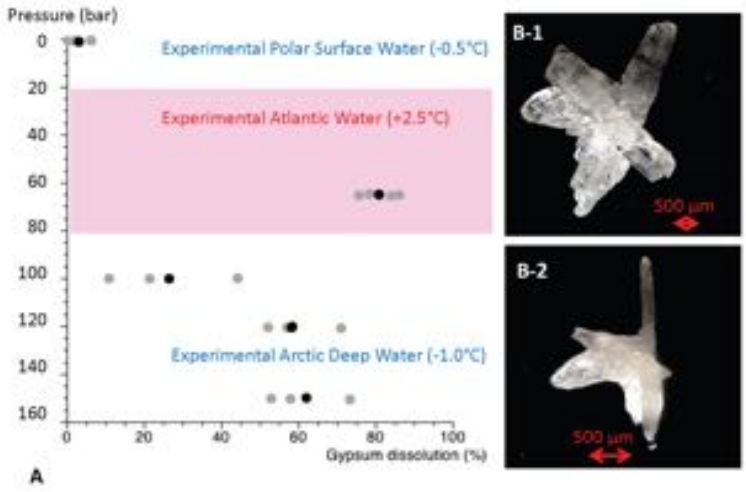

Figure 6: Results from cryogenic gypsum dissolution experiments. A) Graph showing the position of the simulated Arctic water masses in respect to pressure and temperature and how much gypsum (%) was dissolved on average over a 24-hours lasting exposure to such pressure and temperature conditions. Grey dots indicate the values from each aquarium, black dots the mean per experiment. B-1) Cryogenic gypsum crystal of the 120 bar-experiment

887 before exposure. B-2) The same cryogenic gypsum crystal of the 120 bar-experiment after 24
888 hours.
889
890

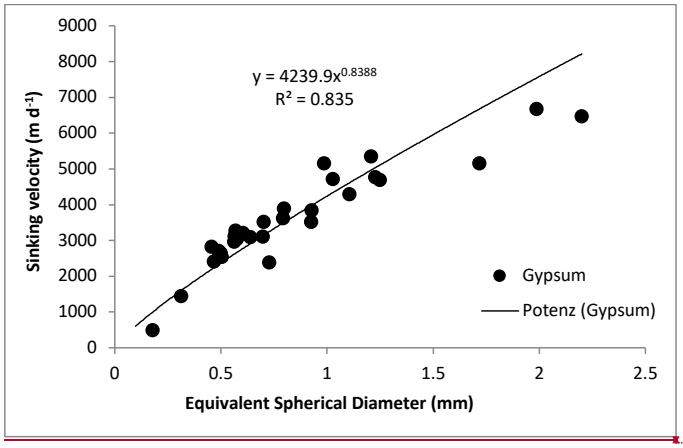

Fig. 7: Sinking velocity of cryogenic gypsum crystals plotted against equivalent spherical diameter (ESD).

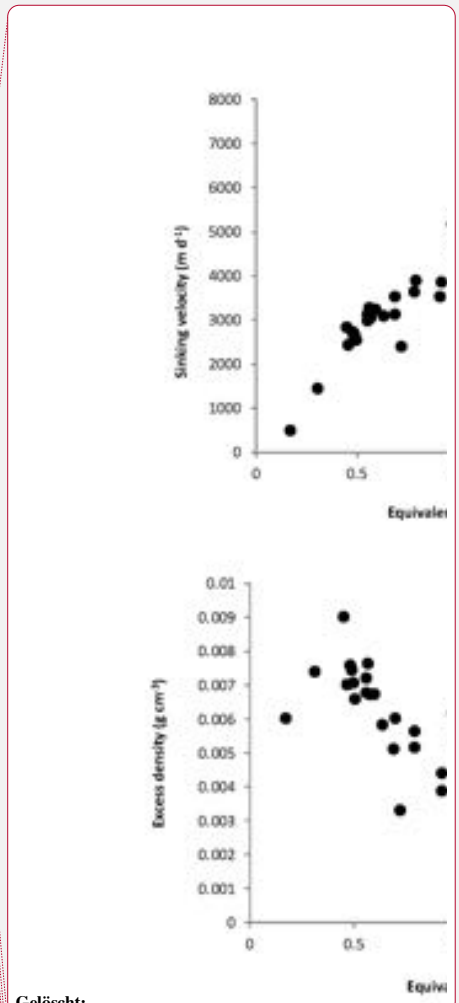

Gelöscht:

Formatiert: Deutsch

Gelöscht: (A) sinking

Gelöscht: and (B) excess density (excess density = gypsum density – seawater density)

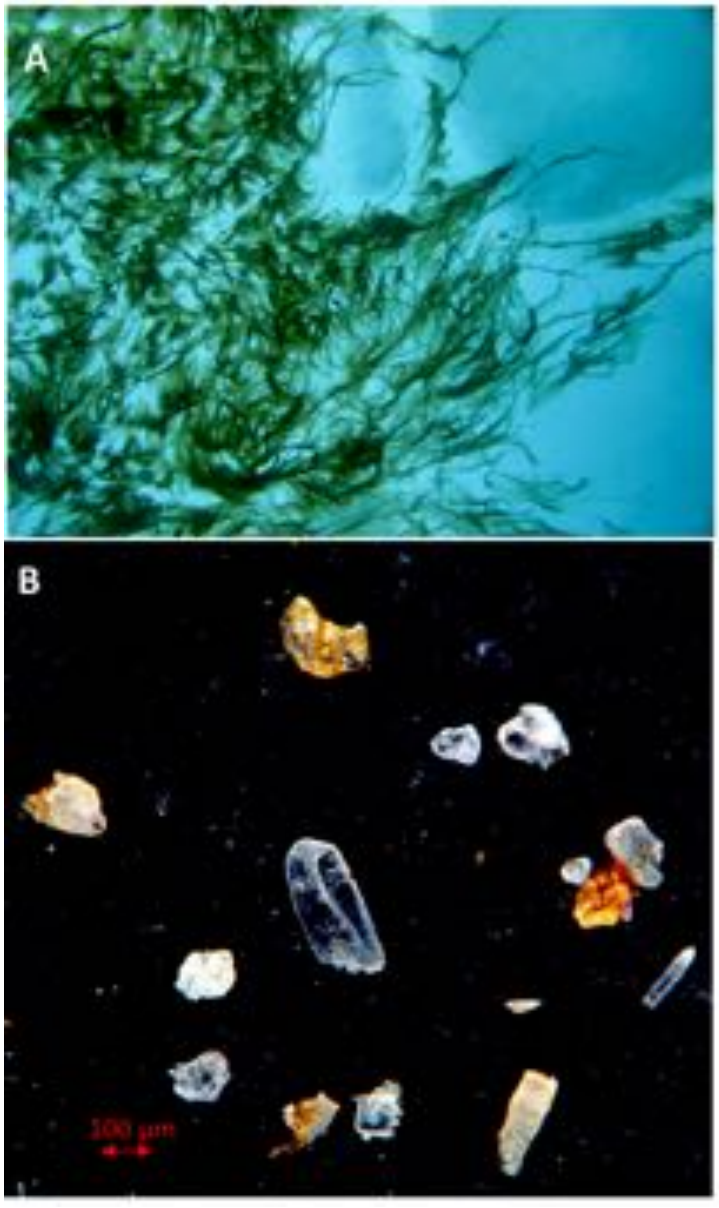

899

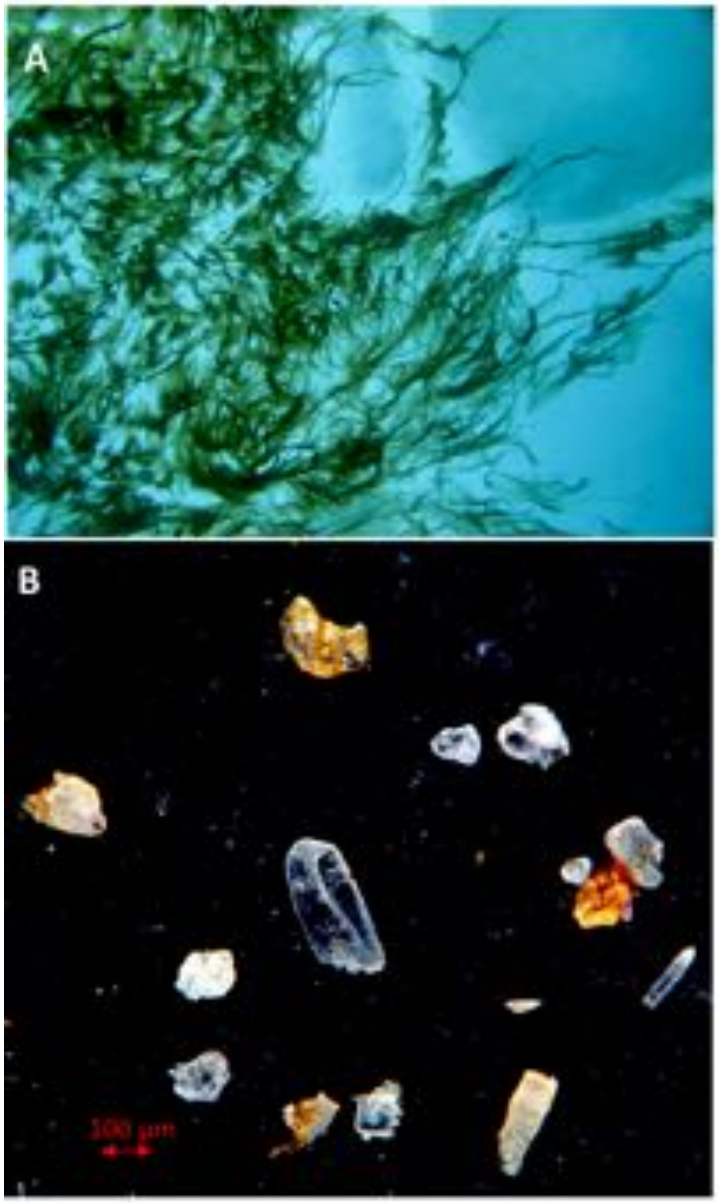

Fig. 8: Living *Melosira arctica* curtains hanging from ice flows during the PS106 expedition (photo taken by M. Nicolaus and C. Katlein). Cryogenic gypsum isolated from *Melosira arctica* (PS106-1, station 21(Peeken, 2018)).

Acknowledgement:

We thank Gernot Nehrke for performing Raman Spectroscopy on crystals from all catches. Christoph Vogt and Dieter Wolf-Gladrow made valuable comments on the manuscript. We thank the captain and crew of RV Polarstern expedition PS106 for their support at sea. This study was funded by the PACES (Polar Regions and Coasts in a Changing Earth System) Program of the Helmholtz Association, the Helmholtz Infrastructure Fund "Frontiers in Arctic Marine Monitoring (FRAM)". This study used samples and data provided by the Alfred-Wegener-Institut Helmholtz-Zentrum für Polar- und Meeresforschung in Bremerhaven from *Polarstern* expedition PS 106 (Grant No. AWI-PS106_00).

Author Contributions:

J.W., H.F: and M.I. designed this study. J.W. lead the writing of this manuscript and performed gypsum sample preparation and analysis. H.F., I.P., C.K., G.C., M.N. acquired ROVnet and ice samples in the field. M.I. measured crystal settling velocities. T.K. performed the backtracking analysis. All authors contributed to the writing and editing of the manuscript.

Gelöscht: and we thank them very much for it.

Formatiert: Zeilenabstand: 1.5 Zeilen

Gelöscht: as well as

Gelöscht: ¶
¶
¶
¶
¶
¶

Seite 24: [1] Gelöscht **change** **03.04.20 12:21:00**